

Chapter 2

Coexistence of Cluster States and Mean-Field-Type States

Hisashi Horiuchi

2.1 Introduction

The saturation property of binding energy and density of the nucleus means that nucleons are easy to assemble and disassemble. If we regard nuclear clustering as being the physics of dynamical assembling and disassembling of nucleons, clustering is a basic nuclear dynamics and appears abundantly in many problems of nuclear structure and reactions [1, 2]. We can say that the formation of clusters is a fundamental aspect of nuclear many body dynamics together with the formation of mean field.

The omnipresence of cluster dynamics in nuclei has long been reported in various phenomena as has been discussed in many conferences and many review papers [3–8]. One of the most impressive manifestations of the omnipresence of clustering has recently been obtained through the studies of neutron-rich unstable nuclei. We now know that neutron-rich nuclei present us with novel types of cluster structure which are composed of clusters and many valence neutrons. Participation of excess neutrons as basic constituents of cluster structure gives rise to quite different features from the cluster structure in stable nuclei.

The coexistence of two structures, the cluster structure and the mean-field-type structure, which are very different to each other, is a unique feature of nuclear system. The coexistence implies that the nuclear many-body physics contains the physics of the structure change between two very distinct structures. We need to clarify what is the relation between two different structures and how one type of structure changes into the other type of structure.

H. Horiuchi (✉)

Research Center for Nuclear Physics, Osaka University,
Osaka 567-0047, Japan
e-mail: horiuchi@rcnp.osaka-u.ac.jp

International Institute for Advanced Studies,
Kizugawa 619-0225, Japan

The purpose of this lecture is to discuss two fundamental problems of nuclear cluster physics: (1) how are the coexistence features of cluster states and mean-field-type states in nuclei?, (2) how does nuclear structure change from shell-model-like ground state to cluster states? Our discussion in this lecture is, however, restricted only to stable nuclei. Namely, we do not discuss the dynamics due to the excess neutrons in this lecture.

In this lecture I first review some of the present understandings of the first problem, which is the main purpose of this lecture. This review is made in two parts. In the first part I discuss the relation of cluster structure and deformed mean-field-type structure in p -shell and light sd -shell nuclei. In the second part I discuss the coexistence of cluster structure and superdeformation in sd -shell and light pf -shell nuclei. Specifically, in the first part I discuss the coexistence features of mean-field-type structure and typical cluster structures in ${}^8\text{Be}$, ${}^{12}\text{C}$, ${}^{16}\text{O}$, and ${}^{20}\text{Ne}$. In the second part, I discuss the coexistence features in ${}^{44}\text{Ti}$ and ${}^{32}\text{S}$. The investigation in ${}^{32}\text{S}$ suggests strong interrelation of ${}^{16}\text{O} + {}^{16}\text{O}$ molecular states and superdeformed states. For the discussions of ${}^{20}\text{Ne}$, ${}^{44}\text{Ti}$ and ${}^{32}\text{S}$ systems, I utilize the results of the detailed studies with antisymmetrized molecular dynamics (AMD).

I then discuss the second problem, the mechanism of the structure-change between cluster structure and mean-field-type structure. The discussion is made on the basis of the studies of the above two subjects about the coexistence features. I argue that the structure change and the resulting coexistence come from the dual nature of nuclear wave functions which have both characters of cluster wave function and mean-field-type wave function. This argument is shown to be supported by the analyses of the electric monopole ($E0$) transitions between cluster states and the ground state which are reported recently in the cases of ${}^{16}\text{O}$ and ${}^{12}\text{C}$.

2.2 AMD Theory

Since in this lecture we often use the results of AMD calculations, we give here a brief explanation of the AMD model.

2.2.1 AMD Wave Function

The basic building block of the AMD wave function is a Slater determinant

$$\Phi_{\text{int}} = \frac{1}{\sqrt{A!}} \det\{\varphi_1, \varphi_2, \dots, \varphi_A\}, \quad (2.1)$$

$$\varphi_i(r) = \phi_i(r) \chi_i \xi_i, \quad \phi_i(r) \propto \exp\left\{-\sum_{\sigma=x,y,z} v_{\sigma}(r_{\sigma} - Z_{i\sigma})^2\right\}, \quad (2.2)$$

$$\chi_i = \alpha_i \chi_{i\uparrow} + \beta_i \chi_{i\downarrow}, \quad |\alpha_i|^2 + |\beta_i|^2 = 1, \quad \xi_i = \text{proton or neutron.} \quad (2.3)$$

The parameter $\{Z_{i\sigma}\}$ is a complex vector whose real part $\text{Re}(Z_{i\sigma})$ gives the spatial position of the Gaussian wave packet $\phi_i(r)$ while imaginary part $\text{Im}(Z_{i\sigma})$ gives the momentum of the packet. The imaginary part of $Z_{i\sigma}$ is important to take into account of the effect of the two-nucleon spin-orbit interaction. The size parameter v_σ can take different values for different spatial directions $\sigma = x, y, z$ but takes common value for all the nucleons usually. The Slater determinant Φ_{int} remains unchanged for any linear transformation of single nucleon wave functions, $\{\varphi_1, \varphi_2, \dots, \varphi_A\} \rightarrow \{\varphi'_1, \varphi'_2, \dots, \varphi'_A\}$ with $\varphi'_i = \sum_{j=1}^A T_{ij} \varphi_j$; namely $\Phi_{\text{int}}(\{\varphi_i\}) = \det\{T\} \Phi_{\text{int}}(\{\varphi'_i\})$. Therefore, for example, we can replace φ_1 and φ_2 by $(\varphi_1 + \varphi_2)$ and $(\varphi_1 - \varphi_2)$ by keeping Φ_{int} unchanged. If two wave packets φ_1 and φ_2 are located at almost the same spatial positions $\text{Re}(Z_{1\sigma}) \approx \text{Re}(Z_{2\sigma})$ with zero momenta $\text{Im}(Z_{1\sigma}) = \text{Im}(Z_{2\sigma}) = 0$, $(\varphi_1 + \varphi_2)$ and $(\varphi_1 - \varphi_2)$ are almost equal to the $0s$ and $0p$ wave functions, respectively, around the spatial position $\text{Re}(Z_{1\sigma}) \approx \text{Re}(Z_{2\sigma})$. From this argument, we know that the AMD Slater determinant can be almost equal to various kinds of shell model wave functions.

The wave function Φ_{int} is always projected to a good-parity wave function Φ^\pm ,

$$\Phi^\pm = (1 \pm P) \Phi_{\text{int}}. \quad (2.4)$$

The parameters of Φ^\pm , v_σ , $Z_{i\sigma}$, α_i , and β_i , are determined by energy variation under the constraint of the given value of the quadrupole deformation parameter β_0 , and such wave function Φ^\pm is denoted as $\Phi^\pm(\beta_0)$. From $\Phi^\pm(\beta_0)$, we project out good-spin wave functions which are denoted as $\Phi_{MK}^{J\pm}$,

$$\begin{aligned} \Phi_{MK}^{J\pm}(\beta_0) &= P_{MK}^J \Phi^\pm(\beta_0) \\ &= \int_0^{2\pi} d\alpha \int_0^\pi d\beta \sin \beta \int_0^{2\pi} d\gamma (D_{MK}^J(\alpha, \beta, \gamma))^* \\ &\quad \times \exp(-i\alpha J_z) \exp(-i\beta J_y) \exp(-i\gamma J_z) \Phi^\pm(\beta_0), \end{aligned} \quad (2.5)$$

where $D_{MK}^J(\alpha, \beta, \gamma)$ is Wigner's D function given as

$$D_{MK}^J(\alpha, \beta, \gamma) = \langle JM | \exp(-i\alpha J_z) \exp(-i\beta J_y) \exp(-i\gamma J_z) | JK \rangle. \quad (2.6)$$

The AMD wave function $\Phi_n^{J\pm}$ is obtained by superposing $\Phi_{MK}^{J\pm}(\beta_0)$ with various values of β_0 ,

$$\Phi_n^{J\pm} = c_n \Phi_{MK}^{J\pm}(\beta_0) + c'_n \Phi_{MK}^{J\pm}(\beta'_0) + \dots \quad (2.7)$$

The superposition coefficients, c_n , c'_n , and so on, are determined by energy variation.

2.2.2 Hartree–Fock-Type Orbits

From the intrinsic wave function of AMD Φ_{int} , we can extract the single nucleon orbits of Hartree–Fock type by which we can study mean-field character of the AMD wave function [9, 10]. First we orthonormalize the single nucleon wave packets φ_i ,

$$\hat{\varphi}_\alpha = \frac{1}{\sqrt{\mu_\alpha}} \sum_{j=1}^A d_{j\alpha} \varphi_j, \quad \sum_{j=1}^A \langle \varphi_i | \varphi_j \rangle d_{j\alpha} = \mu_\alpha d_{i\alpha}. \quad (2.8)$$

Next we construct the Hartree–Fock single nucleon Hamiltonian h by this orthonormalized basis, which takes the following form when the inter-nucleon interaction consists of only two-body force \hat{v}

$$h_{\alpha\beta} = \langle \hat{\varphi}_\alpha | \hat{t} | \hat{\varphi}_\beta \rangle + \sum_\gamma \langle \hat{\varphi}_\alpha \hat{\varphi}_\gamma | \hat{v} | \hat{\varphi}_\beta \hat{\varphi}_\gamma - \hat{\varphi}_\gamma \hat{\varphi}_\beta \rangle. \quad (2.9)$$

The single nucleon orbit ψ_p and its single nucleon energy e_p of Hartree–Fock type are obtained by diagonalizing $h_{\alpha\beta}$ as

$$\psi_p = \sum_\alpha g_{\alpha p} \hat{\varphi}_\alpha, \quad \sum_\beta h_{\alpha\beta} g_{\beta p} = e_p g_{\alpha p}. \quad (2.10)$$

Since the Hartree–Fock type orbits $\{\psi_1, \psi_2, \dots, \psi_A\}$ are obtained by linear transformation of $\{\varphi_1, \varphi_2, \dots, \varphi_A\}$, we have

$$\frac{1}{\sqrt{A!}} \det\{\psi_1, \psi_2, \dots, \psi_A\} \propto \frac{1}{\sqrt{A!}} \det\{\varphi_1, \varphi_2, \dots, \varphi_A\} = \Phi_{\text{int}}. \quad (2.11)$$

2.3 Coexistence of Cluster Structure and Deformed Mean-Field-Type Structure in p -Shell and Light sd -Shell Nuclei

Coexistence features of cluster states and mean-field-type states have been studied in many nuclei. In this lecture I review representative examples of such studies in two parts. In this section I discuss the first part which is for the relation of cluster structure and deformed mean-field-type structure in p -shell and light sd -shell nuclei specifically in ^8Be , ^{12}C , ^{16}O , and ^{20}Ne . In the next section I will discuss the second part which is for the coexistence of cluster structure and superdeformation in sd -shell and light pf -shell nuclei, specifically in ^{44}Ti and ^{32}S . In the cases of discussions of ^{20}Ne , ^{44}Ti , and ^{32}S , I utilize the results of the detailed AMD calculations of the coexistence features.

2.3.1 ^8Be Case

2.3.1.1 Brink Wave Function and its Relation to Shell-Model Wave Function

The $\alpha + \alpha$ structure of ^8Be has long been investigated by many authors as the most fundamental two-cluster structure. The intrinsic wave function of the Brink model [11] for ^8Be with $\alpha + \alpha$ structure is given as

$$\begin{aligned}\Psi(d) &= n_0(d) \mathcal{A} \left\{ \psi\left(\alpha_1, \frac{d}{2} e_z\right) \psi\left(\alpha_2, -\frac{d}{2} e_z\right) \right\} \\ &= \frac{n_0(d)}{\sqrt{4!4!}} \det \left\{ g\left(r_1 - \frac{d}{2} e_z, v\right) \chi_{\uparrow} \xi_p \times \cdots \times g\left(r_4 - \frac{d}{2} e_z, v\right) \chi_{\downarrow} \xi_n \right. \\ &\quad \left. \times g\left(r_5 + \frac{d}{2} e_z, v\right) \chi_{\uparrow} \xi_p \times \cdots \times g\left(r_8 + \frac{d}{2} e_z, v\right) \chi_{\downarrow} \xi_n \right\},\end{aligned}\quad (2.12)$$

$$\begin{aligned}\psi(\alpha_k, a) &= \frac{1}{\sqrt{4!}} \det \left\{ (g(r - a, v))^4 \right\} \quad (r = r_{k_0+1} \sim r_{k_0+4}) \\ &= \frac{1}{\sqrt{4!}} \det \left\{ g(r_{k_0+1} - a, v) \chi_{\uparrow} \xi_p \times \cdots \times g(r_{k_0+4} - a, v) \chi_{\downarrow} \xi_n \right\}, \\ &\quad \{k_0 = 4(k-1)\}\end{aligned}\quad (2.13)$$

$$g(r, \gamma) = \left(\frac{2\gamma}{\pi}\right)^{3/4} \exp(-\gamma r^2), \quad (2.14)$$

where \mathcal{A} is the antisymmetrizing operator of nucleons belonging to different α clusters, $n_0(d)$ is the normalization constant and e_z is a unit vector along the z -direction. $n_0(d)$ is calculated by the relation

$$\begin{aligned}1 &= \langle \Psi(d) | \Psi(d) \rangle \\ &= \left(\frac{n_0(d)}{\sqrt{4!4!}} \right)^2 8! \left(1 - \langle g(r - \frac{d}{2} e_z, v) | g(r + \frac{d}{2} e_z, v) \rangle^2 \right)^4,\end{aligned}\quad (2.15)$$

which gives us

$$n_0(d) = \sqrt{\frac{4!4!}{8!}} \frac{1}{v^2 d^4 + O(d^6)}. \quad (2.16)$$

In the limit of zero inter- α distance d , $\Psi(d)$ becomes equivalent to the intrinsic wave function of the SU(3) shell model with $(\lambda, \mu) = (4, 0)$;

$$\lim_{d \rightarrow 0} \Psi(d) = \frac{1}{\sqrt{8!}} \det \{ (0, 0, 0)^4 (0, 0, 1)^4 \}, \quad (2.17)$$

where (n_x, n_y, n_z) stands for the single particle wave function of the harmonic oscillator model

$$(n_x, n_y, n_z) = \phi_{n_x}(x, v) \phi_{n_y}(y, v) \phi_{n_z}(z, v), \quad (2.18)$$

$$\begin{aligned} \phi_n(x, v) = \text{one dimensional harmonic oscillator function with} \\ n \text{ quanta and size parameter } v = m\omega/2\hbar. \end{aligned} \quad (2.19)$$

The relation of Eq. (2.17) can be proved by using the expansion of $g(r + (d/2)e_z, v)$ around $g(r - (d/2)e_z, v)$. We introduce the notation $(n_x, n_y, n_z)'$ and $(n_x, n_y, n_z)''$ to express the Cartesian harmonic oscillator function (n_x, n_y, n_z) around the spatial position $(d/2)e_z$ and $-(d/2)e_z$, respectively. Then we have $g(r + (d/2)e_z, v) = (0, 0, 0)''$ and $g(r - (d/2)e_z, v) = (0, 0, 0)'$. We can easily prove the relation

$$(0, 0, 0)'' = \exp\left(-\frac{1}{2}vd^2\right) \left\{ (0, 0, 0)' - \sqrt{v}d(0, 0, 1)' + O(d^2) \right\}, \quad (2.20)$$

where $O(d^2)$ expresses the terms of d^2 and higher order terms of d than d^2 . The insertion of this relation together with Eq. (2.16) into $\Psi(d)$ gives us the proof of Eq. (2.17).

2.3.1.2 Bayman–Bohr Theorem

A useful way to relate the Brink wave function $\Psi(d)$ to the shell-model wave function is given by expressing $\Psi(d)$ in terms of internal α -cluster wave function $\phi(\alpha)$ and inter-cluster relative wave function $\Gamma(r_{\alpha\alpha}, d)$,

$$\begin{aligned} \Psi(d) &= n_0(d) \mathcal{A} \left\{ \psi(\alpha_1, \frac{d}{2}e_z) \psi\left(\alpha_2, -\frac{d}{2}e_z\right) \right\} \\ &= n_0(d) \mathcal{A} \{ \Gamma(r_{\alpha\alpha}, d) \phi(\alpha_1) \phi(\alpha_2) \} g(X_G, 8v), \end{aligned} \quad (2.21)$$

$$\Gamma(r_{\alpha\alpha}, d) = g(r_{\alpha\alpha} - de_z, 2v) = \left(\frac{4v}{\pi}\right)^{3/4} \exp(-2v(r_{\alpha\alpha} - de_z)^2), \quad (2.22)$$

$$g(X_G, 8v) = \left(\frac{16v}{\pi}\right)^{3/4} \exp(-8v(X_G)^2), \quad (2.23)$$

$$r_{\alpha\alpha} = X_1 - X_2, \quad X_G = \frac{1}{2}(X_1 + X_2) = \frac{1}{8} \sum_{i=1}^8 r_i, \quad (2.24)$$

$$X_1 = \frac{1}{4} \sum_{i=1}^4 r_i, \quad X_2 = \frac{1}{4} \sum_{i=5}^8 r_i. \quad (2.25)$$

Here we used the relation

$$\psi(\alpha_k, a) = \left(\frac{8v}{\pi}\right)^{3/4} \exp(-4v(X_k - a)^2) \phi(\alpha_k). \quad (2.26)$$

The actual form of the inter- α relative wave function $\Gamma(r_{\alpha\alpha}, d)$ deviates from the Gaussian wave packet due of the effect of the antisymmetrization. The effect of the antisymmetrization is well reflected in the following relation,

$$\mathcal{A} \left\{ X_{(n_x, n_y, n_z)}(r_{\alpha\alpha}, 2v) \phi(\alpha_1) \phi(\alpha_2) \right\} = 0, \quad \text{for } n_x + n_y + n_z < 4, \quad (2.27)$$

where $X_{(n_x, n_y, n_z)}(r, \gamma)$ stands for the Cartesian harmonic oscillator function defined as $X_{(n_x, n_y, n_z)}(r, \gamma) = \phi_{n_x}(x, \gamma) \phi_{n_y}(y, \gamma) \phi_{n_z}(z, \gamma)$. It is to be noted that, for $\gamma = v$, $X_{(n_x, n_y, n_z)}(r, \gamma)$ is equal to (n_x, n_y, n_z) defined before. Eq. (2.27) is easy to understand. We first notice the following relation

$$\begin{aligned} N_{\text{op}} \mathcal{A} \left\{ X_{(n_x, n_y, n_z)}(r_{\alpha\alpha}, 2v) \phi(\alpha_1) \phi(\alpha_2) \right\} X_{(0,0,0)}(X_G, 8v) \\ = (n_x + n_y + n_z) \mathcal{A} \left\{ X_{(n_x, n_y, n_z)}(r_{\alpha\alpha}, 2v) \phi(\alpha_1) \phi(\alpha_2) \right\} X_{(0,0,0)}(X_G, 8v), \end{aligned} \quad (2.28)$$

where $X_{(0,0,0)}(X_G, 8v) = (16v/\pi)^{3/4} \exp(-8v(X_G)^2) = g(X_G, 8v)$ and N_{op} stands for the total number operator of harmonic oscillator quanta. Eq. (2.28) is verified to hold by noting the following relation

$$(N_{\text{op}})_\sigma = \sum_{i=1}^8 (N_{\text{op}}(i))_\sigma = (N_{\text{op}}(\alpha_1))_\sigma + (N_{\text{op}}(\alpha_2))_\sigma + (N_{\text{op}}(r_{\alpha\alpha}))_\sigma + (N_{\text{op}}(X_G))_\sigma, \quad (2.29)$$

$$(N_{\text{op}}(\alpha_1))_\sigma = \sum_{i=1}^4 (N_{\text{op}}(i))_\sigma - (N_{\text{op}}(X_1))_\sigma, \quad = \sum_{i=5}^8 (N_{\text{op}}(i))_\sigma - (N_{\text{op}}(X_2))_\sigma, \quad (2.30)$$

$$(N_{\text{op}}(X_1))_\sigma + (N_{\text{op}}(X_2))_\sigma = (N_{\text{op}}(r_{\alpha\alpha}))_\sigma + (N_{\text{op}}(X_G))_\sigma \quad (2.31)$$

$$\begin{aligned} (N_{\text{op}}(i))_\sigma = N((r_i)_\sigma, m), \quad (N_{\text{op}}(r_{\alpha\alpha}))_\sigma = N(r_{\alpha\alpha})_\sigma, 2m), \quad (N_{\text{op}}(X_G))_\sigma = N(X_G)_\sigma, 8m), \\ (N_{\text{op}}(X_k))_\sigma = N((X_k)_\sigma, 4m) \quad X_1 = \frac{1}{4} \sum_{i=1}^4 r_i, \quad X_2 = \frac{1}{4} \sum_{i=5}^8 r_i, \end{aligned} \quad (2.32)$$

$$N(r, \mu) = \frac{1}{\hbar\omega} \left(\frac{-\hbar^2}{2\mu} \left(\frac{\partial}{\partial r} \right)^2 + \frac{\mu\omega^2}{2} r^2 \right) - \frac{3}{2}, \quad (2.33)$$

$$\begin{aligned}
N_{\text{op}} &= \sum_{\sigma=x,y,z} (N_{\text{op}})_{\sigma}, \quad N_{\text{op}}(i) = \sum_{\sigma=x,y,z} (N_{\text{op}}(i))_{\sigma}, \quad N_{\text{op}}(r_{\alpha\alpha}) = \sum_{\sigma=x,y,z} (N_{\text{op}}(r_{\alpha\alpha}))_{\sigma}, \\
N_{\text{op}}(X_G) &= \sum_{\sigma=x,y,z} (N_{\text{op}}(X_G))_{\sigma}, \quad N_{\text{op}}(\alpha_k) = \sum_{\sigma=x,y,z} (N_{\text{op}}(\alpha_k))_{\sigma}.
\end{aligned} \tag{2.34}$$

Since $N_{\text{op}}(\alpha)\phi(\alpha) = N_{\text{op}}(X_G)X_{(0,0,0)}(X_G, 8v) = 0$, there holds Eq. (2.28). Now, the shell model teaches us that the lowest number of the total oscillator quanta of ${}^8\text{Be}$ is 4, which is given by $\det\{(0s)^4(0p)^4\}$. Therefore we have

$$\mathcal{A}\left\{X_{(n_x, n_y, n_z)}(r_{\alpha\alpha}, 2v)\phi(\alpha_1)\phi(\alpha_2)\right\}g(X_G, 8v) = 0, \quad \text{for } n_x + n_y + n_z < 4, \tag{2.35}$$

from which there follows Eq. (2.27).

By using the expansion of $\Gamma(r_{\alpha\alpha}, d)$ with the harmonic oscillator basis functions, $\Gamma(r_{\alpha\alpha}, d) = \exp(-vd^2) \sum_{n=0}^{\infty} \{(\sqrt{2vd})^n / \sqrt{n!}\} X_{(0,0,n)}(r_{\alpha\alpha}, 2v)$, we obtain

$$\begin{aligned}
\Psi(d) &= n_0(d) \mathcal{A}\{\Gamma(r_{\alpha\alpha}, d)\phi(\alpha_1)\phi(\alpha_2)\}g(X_G, 8v) \\
&= n_0(d) \exp(-vd^2) \left\{ \frac{(\sqrt{2vd})^4}{\sqrt{4!}} \mathcal{A}\{X_{(0,0,4)}(r_{\alpha\alpha}, 2v)\phi(\alpha_1)\phi(\alpha_2)\} + O(d^6) \right\} \\
&\quad \times g(X_G, 8v),
\end{aligned} \tag{2.36}$$

where we used Eq. (2.27). From this relation we obtain

$$\lim_{d \rightarrow 0} \Psi(d) = C_0 \mathcal{A}\{X_{(0,0,4)}(r_{\alpha\alpha}, 2v)\phi(\alpha_1)\phi(\alpha_2)\}g(X_G, 8v), \tag{2.37}$$

where $C_0 = 4\sqrt{4!/8!} = 1/\sqrt{7!!}$. By combining this with Eq. (2.17) we obtain

$$\begin{aligned}
&\frac{1}{\sqrt{8!}} \det\{(0, 0, 0)^4(0, 0, 1)^4\} \\
&= C_0 \mathcal{A}\{X_{(0,0,4)}(r_{\alpha\alpha}, 2v)\phi(\alpha_1)\phi(\alpha_2)\}g(X_G, 8v).
\end{aligned} \tag{2.38}$$

This relation is known as an example of the relations of Bayman–Bohr theorem [12] which says that the SU(3) shell model wave function of the ground state is in most cases equivalent to the cluster model wave function. Eq. (3.38) can be proved more directly by noticing that both the left-side and right-side wave functions are the eigenstates of $(N_{\text{op}})_x$, $(N_{\text{op}})_y$, and $(N_{\text{op}})_z$ with eigenvalues 0, 0, 4, respectively. Since it is evident that there is only one wave function of ${}^8\text{Be}$ which is an eigenstate of $(N_{\text{op}})_x$, $(N_{\text{op}})_y$, and $(N_{\text{op}})_z$ with eigenvalues 0, 0, 4, respectively, the right-side cluster wave function of Eq. (3.38) is necessarily equal to the left-side wave function. By applying the angular momentum projection to Eq. (3.38), we get the Bayman–Bohr theorem written in the form of good angular momentum states,

$$\begin{aligned}
& |(0s)^4(0p)^4, (\lambda, \mu) = (4, 0)LM\rangle \\
& = C_{0,\mathcal{A}} \{R_{N=4,L}(r_{\alpha\alpha}, 2\nu) Y_{LM}(\hat{r}_{\alpha\alpha}) \phi(\alpha_1) \phi(\alpha_2)\} g(X_G, 8\nu),
\end{aligned} \tag{2.39}$$

where $R_{N,L}(r, \gamma)$ stands for the radial harmonic oscillator function with the size parameter γ and with the number of oscillator quanta N namely with the number of nodes $n = (N - L)/2$.

2.3.1.3 α - α Interaction and Spatial Localization of α Cluster

If the SU(3) shell model description is good for ${}^8\text{Be}$, it means that the inter- α relative wave function in the intrinsic ${}^8\text{Be}$ wave function is well described by the harmonic oscillator function $X_{(0,0,4)}(r_{\alpha\alpha}, 2\nu)$. If the inter- α interaction is strongly attractive, the inter- α relative wave function should express the most compact state allowable by the Pauli principle and hence it is given by $X_{(0,0,4)}(r_{\alpha\alpha}, 2\nu)$. Therefore whether the SU(3) shell model description is good or not for ${}^8\text{Be}$ can be studied by the investigation of the inter- α interaction. The microscopic study of the α - α interaction has a long history [3–5, 13–17]. The essential feature of the α - α interaction is described by the theory of the orthogonality condition model (OCM) which is an approximation of the RGM (resonating group method) approach. The RGM gives us the α - α relative wave function $\chi(r_{\alpha\alpha})$ as the solution of the integro-differential equation

$$\langle \phi(\alpha_1) \phi(\alpha_2) | (H - E) | \mathcal{A} \{ \chi(r_{\alpha\alpha}) \phi(\alpha_1) \phi(\alpha_2) \} \rangle = 0, \tag{2.40}$$

$$H = \sum_{q=1}^8 T_q - T_G + \sum_{q < q'}^8 V_{q,q'}^{(2)}, \tag{2.41}$$

where T_G is the kinetic energy of the total center of mass. The OCM equation of motion which is aimed at describing essential feature of the RGM equation of motion is written as

$$\Lambda \left(\frac{-\hbar^2}{2(2m)} \left(\frac{\partial}{\partial r_{\alpha\alpha}} \right)^2 + V_{\alpha\alpha}(r_{\alpha\alpha}) - (E - 2E_\alpha) \right) \Lambda \hat{\chi}(r_{\alpha\alpha}) = 0, \tag{2.42}$$

where E_α stands for the binding energy of α particle and Λ is the projection operator given as

$$\begin{aligned}
\Lambda &= 1 - \sum_{n_x+n_y+n_z < 4} |X_{(n_x, n_y, n_z)}(r_{\alpha\alpha}, 2\nu)\rangle \langle X_{(n_x, n_y, n_z)}(r_{\alpha\alpha}, 2\nu)| \\
&= 1 - \sum_{N < 4, L, M} |R_{N,L}(r_{\alpha\alpha}, 2\nu) Y_{LM}(\hat{r}_{\alpha\alpha})\rangle \langle R_{N,L}(r_{\alpha\alpha}, 2\nu) Y_{LM}(\hat{r}_{\alpha\alpha})|.
\end{aligned} \tag{2.43}$$

The wave functions $X_{(n_x, n_y, n_z)}(r_{\alpha\alpha}, 2\nu)$ with $n_x + n_y + n_z < 4$ and $R_{N,L}(r_{\alpha\alpha}, 2\nu) Y_{LM}(\hat{r}_{\alpha\alpha})$ with $N < 4$ are called the Pauli-forbidden states because they satisfy the relation of Eq. (2.27) and

$$\mathcal{A}\{R_{N,L}(r_{\alpha\alpha}, 2\nu)Y_{LM}(\hat{r}_{\alpha\alpha})\phi(\alpha_1)\phi(\alpha_2)\} = 0, \quad \text{for } N < 4, \quad (2.44)$$

respectively. The operator Λ projects the relative wave function onto the functional space orthogonal to the Pauli-forbidden states. The local potential $V_{\alpha\alpha}(r_{\alpha\alpha})$ is close to the double folding potential and hence it is deep. Because of Eqs. (2.27) and (2.44), Λ satisfies the relation, $\mathcal{A}\{[A\chi(r_{\alpha\alpha})]\phi(\alpha_1)\phi(\alpha_2)\} = \mathcal{A}\{\chi(r_{\alpha\alpha})\phi(\alpha_1)\phi(\alpha_2)\}$. The wave function $\hat{\chi}(r_{\alpha\alpha})$ is related to $\chi(r_{\alpha\alpha})$ as

$$\hat{\chi}(r_{\alpha\alpha}) = \sqrt{N_K} \chi(r_{\alpha\alpha}), \quad (2.45)$$

where N_K is defined by

$$\langle \phi(\alpha_1)\phi(\alpha_2) | \mathcal{A}\{\chi(r_{\alpha\alpha})\phi(\alpha_1)\phi(\alpha_2)\} \rangle = N_K \chi(r_{\alpha\alpha}). \quad (2.46)$$

N_K and Λ satisfy the relations, $\Lambda N_K = N_K \Lambda = N_K$, $\Lambda \sqrt{N_K} = \sqrt{N_K} \Lambda = \sqrt{N_K}$. In the α - α system, $\sqrt{N_K}$ is close to Λ and hence $\hat{\chi}(r_{\alpha\alpha})$ is close to $\chi(r_{\alpha\alpha})$. The OCM equation of Eq. (2.42) implies that the essential effect of the Pauli principle is expressed by the orthogonalization of the relative wave function to the Pauli-forbidden states. Namely, OCM equation says that the relative wave function is obtained by the deep potential $V_{\alpha\alpha}(r_{\alpha\alpha})$ similar to the double folding potential under the condition of the orthogonality to the Pauli-forbidden states. It was shown that the OCM equation reproduces well the α - α relative wave function $\chi(r_{\alpha\alpha})$ and the α - α scattering phase-shifts given by the RGM equation [13, 14].

The calculated relative wave function $\chi(r_{\alpha\alpha})$ has characteristic features [13–16]. The radial part of $\chi(r_{\alpha\alpha})$ for low energy has $(4 - L)/2$ nodes in the interaction region which are almost energy-independent and its amplitude is fairly small compared with the amplitude in the outer region. The outermost node is at about 2 fm for both $L = 0$ and 2. The existence of nodal points is due to the orthogonality of the relative wave function to the Pauli-forbidden states. The oscillatory behavior of the radial relative wave function in the inner region causes the large amount of the kinetic energy of the relative motion. The small amplitude of the radial relative wave function in the inner region is caused in order to make the contribution of the kinetic energy from the inner region small as much as possible. If the amplitude of the radial relative wave function in the inner region is large, it can gain energy from the deep attractive potential $V_{\alpha\alpha}(r_{\alpha\alpha})$. Therefore the small amplitude of the radial relative wave function in the inner region means that that the repulsive effect due to the orthogonality to the Pauli-forbidden states is larger than the attractive effect of the potential $V_{\alpha\alpha}(r_{\alpha\alpha})$. The small amplitude of the radial relative wave function in the inner region is always obtained so far as the good reproduction of the α - α scattering phase-shifts is to be guaranteed and this feature remains the same in the ground band resonance states of ^8Be . Since the function $R_{N=4,L}(r_{\alpha\alpha}, 2\nu)$ which the SU(3) shell model assigns as the radial α - α relative wave function has even larger amplitude in the inner region than in the outer region, we observe that the SU(3) description of the ^8Be ground band states is not compatible with the α - α scattering data.

2.3.1.4 α -Gas Like Nature of ${}^8\text{Be}$

Recently the 2α structure of ${}^8\text{Be}$ which is the most fundamental two-cluster structure was cast new light [18]. The 0^+ wave function Φ_{0^+} obtained by the GCM (generator coordinate method) calculation, $\Phi_{0^+} = \sum_{ij} f_{ij} P_{J=0} \mathcal{A} \{ \Gamma(r_{\alpha\alpha}, d_j) \phi(\alpha_1) \phi(\alpha_2) \}$, was shown to be almost 100% equivalent to a single 2α wave function $\Phi^{2\alpha\text{THSR}}(\gamma_0)$ which is called 2α THSR wave function [37] and is defined as

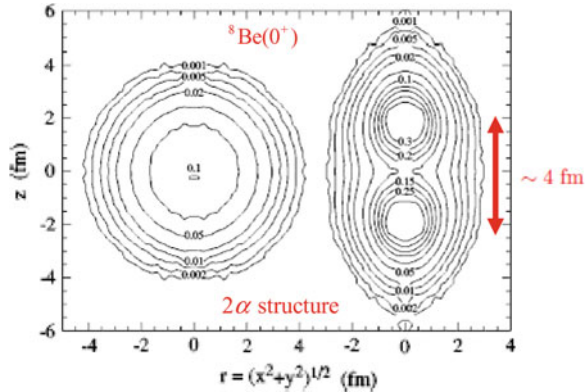
$$\Phi^{2\alpha\text{THSR}}(\gamma_0) = \mathcal{A} \left\{ \exp \left(-2\gamma_0 \sum_{k=1}^2 (X_k - X_G)^2 \right) \phi(\alpha_1) \phi(\alpha_2) \right\}. \quad (2.47)$$

Here $P_{J=0}$ is projection operator of angular momentum onto $J = 0$ and the size parameter γ_0 is much smaller than v . Since the width parameters γ_0 is much smaller than v , α clusters in the THSR wave function are distributed widely in space. By noting that the orthogonality of the α - α relative wave function to Pauli-forbidden states removes the spatially compact components from the relative wave function, we know that the THSR wave function has a very small staying probability of two α clusters in short relative distance region. Small staying probability in the inner region and long tail probability in the outer region of two α clusters is nothing but what the 2α RGM (or OCM) relative wave function $\chi(r_{\alpha\alpha})$ describes.

2.3.1.5 Ab Initio Calculation of ${}^8\text{Be}$

A remarkably important progress in theoretical study of ${}^8\text{Be}$ structure was recently achieved by Wiringa et al [19]. They showed that the wave function of ${}^8\text{Be}$ obtained by their ab initio method with realistic nuclear force has a clear $\alpha + \alpha$ structure with inter- α separation around 4 fm as shown in Fig. 2.1. According to Ref. [19], the net energy contribution from the tensor force to the ${}^8\text{Be}$ binding energy is nearly twice that to ${}^4\text{He}$ binding energy. This result is very plausible for the $\alpha + \alpha$ structure where each α cluster wave function is almost the same as the

Fig. 2.1 Density distribution of ${}^8\text{Be}$ obtained by ab initio calculation (variational Monte Carlo method) [19]



free ^4He wave function with large D-state mixture. It is important to check whether mean-field type wave function can reproduce or not such energy contribution from the tensor force.

2.3.2 ^{12}C Case

2.3.2.1 From Linear-Chain Structure to Gas-Like Structure of 3α for the Hoyle State

The second 0^+ state of ^{12}C is located near the 3α breakup threshold. It is called the Hoyle state [20, 21] in honor of astrophysicist Fred Hoyle who predicted the existence of this state which plays an astrophysically crucial role for the synthesis of ^{12}C in the universe. From the viewpoint of nuclear structure, this state is well known as one of the mysterious 0^+ states in light nuclei. The understanding of its structure has been actually one of the most difficult and challenging problems of nuclear structure. Its small excitation energy of 7.66 MeV has been regarded to be difficult to explain by the shell model. The no-core shell model which is the most advanced modern shell model approach at present has so far not succeeded to reproduce it [22, 23].

More than 40 years ago Morinaga proposed the assignment of 3α linear-chain structure to this Hoyle state [24, 25]. The 3α linear-chain structure is intimately related to the deformed mean-field structure with 4 particle jump from $0p$ shell to $1s0d$ shell;

$$\begin{aligned} & \lim_{d \rightarrow 0} m_0(d) \mathcal{A} \{ \psi(\alpha_1, de_z) \psi(\alpha_2, 0) \psi(\alpha_3, -de_z) \} \\ &= \frac{1}{\sqrt{12!}} \det \{ (0, 0, 0)^4 (0, 0, 1)^4 (0, 0, 2)^4 \}, \end{aligned} \quad (2.48)$$

where $m_0(d)$ is the normalization constant. However the observed reduced α decay width of the Hoyle state is larger than the Wigner limit value and therefore it is contradictory to the linear-chain structure which gives small reduced width. The linear chain structure necessarily contains high partial waves between ^8Be and α clusters in spite of the fact that only the S wave contributes to the α decay because of the small Q value. The 3α linear-chain structure can thus give at most only one third of the Wigner limit value [26]. The reduced α decay width $\theta^2(a)$ deduced from the width $\Gamma_{\text{exp}} = 8.7$ eV of the Hoyle state is given in Table 2.1. The definition of $\theta^2(a)$ is as follows,

Table 2.1 Experimental value of $\theta^2(a)$ of the Hoyle state

a	4.4	4.8	5.2	5.6	6.0
$\theta^2(a)$	2.7	2.2	1.6	1.2	0.9

Channel radius a is in unit of fm

Table 2.2 Calculated value of $\theta^2(a)$ when 3α linear-chain structure is assumed for the Hoyle state

$R_{\alpha\alpha}$	1.0	2.0	3.0	4.0
$\theta^2(a)$	0.29	0.32	0.35	0.37

$R_{\alpha\alpha}$ is the inter- α distance of the chain state, and is in unit of fm

$$\Gamma = 2P_{\ell=0}\theta^2(a)\gamma_W^2(a), \quad P_\ell = \frac{ka}{G_\ell(a) + F_\ell^2(a)}, \quad \gamma_W^2(a) = \frac{3\hbar^2}{2\mu a^2}, \quad (2.49)$$

where a is channel radius, μ reduced mass, and F_ℓ and G_ℓ are regular and irregular Coulomb functions. In terms of reduced width amplitude $y(r)$, we can express $\theta^2(a)$ as $\theta^2(a) = (1/3)a^3y^2(a)$. Note that, in the case of $y(r) = \text{constant}(a \geq r \geq 0)$, $\theta^2(a) = 1$. In Table 2.2 we show the calculated value of $\theta^2(a)$ when 3α linear-chain structure is assumed for the Hoyle state, which is taken from Ref. [26].

The observed large α -decay reduced width of the Hoyle state in the ${}^8\text{Be}(0_1^+) + \alpha$ channel was successfully reproduced by a full three-body OCM calculation [27, 28]. The wave function $\hat{\chi}(\hat{\xi}_1, \hat{\xi}_2)$ of the 3α OCM which should be totally symmetric with respect to the particle permutation is obtained by solving the following equation of motion

$$\left[-\frac{\hbar^2}{2M_\alpha} \sum_{i=1}^3 \left(\frac{\partial}{\partial x_i} \right)^2 - \hat{T}_G + \sum_{i>j}^3 V_{2\alpha}(|x_i - x_j|) - E \right] \hat{\chi}(\hat{\xi}_1, \hat{\xi}_2) = 0, \quad (2.50)$$

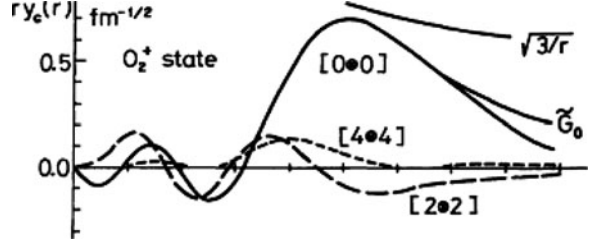
$$\hat{\xi}_1 = x_1 - \frac{1}{2}(x_2 + x_3), \quad \hat{\xi}_2 = x_2 - x_3, \quad (2.51)$$

$$\langle \chi^F(x_i - x_j) | \hat{\chi}(\hat{\xi}_1, \hat{\xi}_2) \rangle = 0, \quad (1 \leq j < i \leq 3). \quad (2.52)$$

The coordinate x_i is the position vector of the i th α cluster. \hat{T}_G is the kinetic energy of the total center of mass. The 2α wave functions χ^F stand for the Pauli forbidden states of the 2α relative motion which we explained in the previous subsection. Namely, χ^F satisfy $\mathcal{A}[\chi^F(X_i - X_j)\phi(\alpha_i)\phi(\alpha_j)] = 0$, with $X_i = (1/4)\sum_{k=I(i)+1}^{I(i)+4} r_k$, $I(i) = 4(i-1)$, where r_k stands for k th nucleon coordinate. The numbers of Pauli-forbidden states are two and one for S and D waves, respectively. The structure of the Hoyle state obtained by this 3α OCM calculation has, as the dominant component of the Hoyle state, the ${}^8\text{Be}(0_1^+) + \alpha$ structure with relative S wave between two clusters, ${}^8\text{Be}(0_1^+)$ and α . Since ${}^8\text{Be}(0_1^+)$ consists of two α clusters weakly coupled in relative S wave, the Hoyle state was concluded to have a weakly coupled 3α structure in relative S waves with large spatial extent. Namely it was regarded as being a gas-like structure of α clusters.

A few years later, this understanding of the structure of the Hoyle state was reported to be confirmed by fully microscopic 3α calculations by two groups, namely the 3α RGM calculations by Kamimura et al. [29, 30] and the 3α GCM calculations by Uegaki et al. [31–33]. The wave functions of the 3α RGM

Fig. 2.2 Reduced width amplitudes of $[L \otimes L]$ channels (${}^8\text{Be}(L) + \alpha(\ell = L)$ channels) of the 0_2^+ state of ${}^{12}\text{C}$ [31–33]



and GCM have the form, $\Phi_J({}^{12}\text{C}) = \mathcal{A}\{\chi_J(\xi_1, \xi_2)\phi(\alpha_1)\phi(\alpha_2)\phi(\alpha_3)\}$ with $\xi_1 = X_1 - \frac{1}{2}(X_2 + X_3)$, and $\xi_2 = X_2 - X_3$. The 3α relative wave function $\chi_J(\xi_1, \xi_2)$ satisfies the following equation of motion

$$\langle \phi(\alpha_1)\phi(\alpha_2)\phi(\alpha_3) | (H - E) | \mathcal{A}\{\chi_J(\xi_1, \xi_2)\phi(\alpha_1)\phi(\alpha_2)\phi(\alpha_3)\} \rangle = 0, \quad (2.53)$$

$$H = \sum_{q=1}^{12} T_q - T_G + \sum_{q < q'}^{12} V_{q,q'}^{(2)}, \quad (2.54)$$

where T_G is the kinetic energy of the total center of mass. It is to be noted that, due to the Bayman–Bohr theorem, the $\text{SU}(3)$ shell model wave function $|(0s)^4(0p)^8, (\lambda, \mu) = (04)J = 0\rangle$ can be expressed by the 3α cluster wave function,

$$\begin{aligned} |(0s)^4(0p)^8, (\lambda, \mu) = (04)J = 0\rangle \\ = N_0 \mathcal{A}\{R_{4,0}(\xi_1, (8/3)v)R_{4,0}(\xi_2, 2v)\phi(\alpha_1)\phi(\alpha_2)\phi(\alpha_3)\} \\ \times g(X_G, 12v). \end{aligned} \quad (2.55)$$

Figure 2.2 shows that the obtained wave function supports the dominance of ${}^8\text{Be}(0_1^+) + \alpha$ (S wave) structure of the Hoyle state. The reduced width amplitude $y_c(r)$ in this figure is defined as

$$y_{c=(L,\ell)}(r) = \sqrt{\frac{12!}{4!8!}} \left\langle \frac{\delta(\xi_1 - r)}{r^2} \left[\phi_L({}^8\text{Be}) Y_\ell(\hat{\xi}_1) \right]_J \phi(\alpha_1) | \Phi_J({}^{12}\text{C}) \right\rangle. \quad (2.56)$$

These calculations nicely reproduced not only the energy position of the Hoyle state but also other experimental properties including inelastic electron form factor and $E0$ and $E2$ transition properties. In Table 2.3 we show the good reproduction of the ${}^{12}\text{C}$ data by 3α calculation.

2.3.2.2 AMD and FMD + UCOM Calculations

About 20 years later after the 3α calculations of Refs. [29, 30] and [31–33], the results by these microscopic 3α cluster model calculations were confirmed by the antisymmetrized molecular dynamics (AMD) calculation [34] which does not

Table 2.3 Reproduction of the ^{12}C data by 3α calculation of Ref. [29, 30]

	Exp.	Theor.
Excitation energy (0_2^+) (MeV)	7.65	7.74
Width (0_2^+) (eV)	8.7 ± 2.7	7.7
$M(0_2^+ \rightarrow 0_1^+)$ (fm 2)	5.4 ± 0.2	6.7
$B(E2 : 0_2^+ \rightarrow 2_1^+)$ (e 2 fm 4)	13 ± 4	5.6
$B(E2 : 2_1^+ \rightarrow 0_1^+)$ (e 2 fm 4)	7.8	9.3
$R_{\text{rms}}(0_1^+)$ (fm)	2.43	2.4
$R_{\text{rms}}(0_2^+)$ (fm)		3.37

assume the alpha clustering. Figure 2.3 shows the energy spectra and density distributions of obtained states by AMD. Furthermore recently the fermionic molecular dynamics (FMD) calculations [35, 36] gave us quite similar results as the AMD results. This FMD approach which also does not assume the alpha clustering starts from a realistic bare N - N force by using the unitary correlation operator method (UCOM) technique. Since both AMD and FMD+UCOM do not assume alpha clustering but build up wave functions totally on nucleonic degrees of freedom, the obtained wave functions contain components with broken spatial symmetry. Table 2.4 shows the good reproduction by the AMD calculation of the observed β^+ decay strengths to ^{12}C states from the ground 1^+ state of ^{12}N which are due to the components with broken spatial symmetry of ^{12}C wave function.

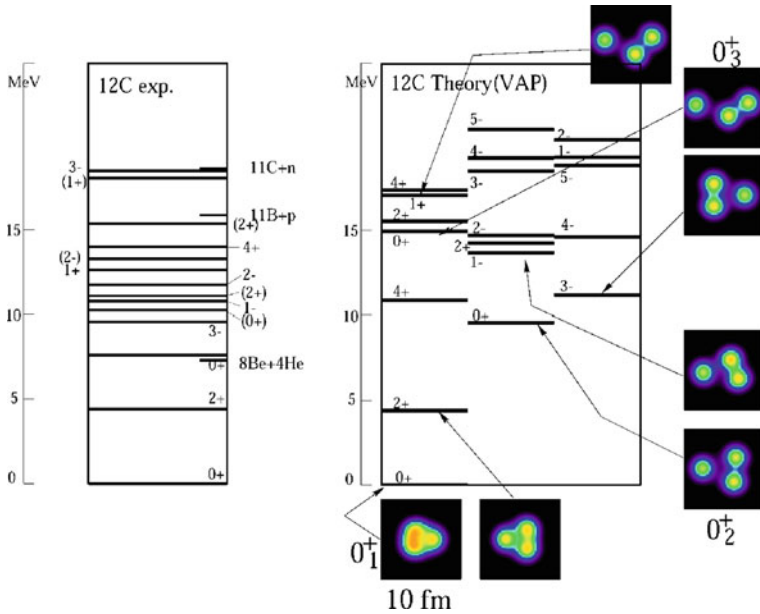
**Fig. 2.3** Energy spectra and density distributions of ^{12}C by AMD [34]

Table 2.4 The experimental data for β decays $^{12}\text{N}(\beta^+)^{12}\text{C}$ compared with the AMD results

States in ^{12}C (MeV)	J^\pm	$(\log ft)_{\text{exp}}$	$(\log ft)_{\text{AMD}} (J_f^\pm)$
0	0^+	4.120 ± 0.003	3.8
4.44	2^+	5.149 ± 0.007	4.8 (2_1^+)
7.65	0^+	4.34 ± 0.06	4.0 (0_2^+)
10.3	(0^+)	4.36 ± 0.17	4.7 (0_3^+)
12.71	1^+	3.52 ± 0.14	3.8 (1_1^+)

2.3.2.3 3α -BEC-Like Structure of the Hoyle State

Almost 30 years after the first proposal of the $^8\text{Be}(0_1^+) + \alpha$ structure for the Hoyle state, this state was reconsidered in a new light in Ref. [37]. The authors of this paper presented, for the description of the Hoyle state, the following new model wave function $\Phi^{3\alpha\text{THSR}}(B)$ which is called the 3α THSR wave function :

$$\begin{aligned} \Phi^{3\alpha\text{THSR}}(B) &= \mathcal{A} \left\{ \exp \left[-\frac{2}{B^2} (X_1^2 + X_2^2 + X_3^2) \right] \phi(\alpha_1) \phi(\alpha_2) \phi(\alpha_3) \right\} \\ &= \exp \left(-\frac{6}{B^2} \zeta_3^2 \right) \mathcal{A} \left\{ \exp \left(-\frac{4}{3B^2} \zeta_1^2 - \frac{1}{B^2} \zeta_2^2 \right) \phi(\alpha_1) \phi(\alpha_2) \phi(\alpha_3) \right\}, \end{aligned} \quad (2.57)$$

where $\zeta_3 = \frac{1}{3}(X_1 + X_2 + X_3)$. As shown in Eq. (2.57), the THSR wave function can be regarded as expressing the cluster structure where the α_1 cluster and a $^8\text{Be}(0_1^+)$ -like cluster $\mathcal{A} \{ \exp(-(1/B^2)\zeta_2^2) \phi(\alpha_2) \phi(\alpha_3) \}$ couple via S -wave with inter-cluster wave function $\exp(-(4/3B^2)\zeta_1^2)$. On the other hand, Eq. (2.57) shows that the THSR wave function represents the state where three α clusters occupy the same single $0S$ -orbit $\exp(-(2/B^2)X^2)$, namely a 3α -condensate-like state which is the finite size counterpart of the macroscopic α -particle Bose–Einstein condensation (BEC) in infinite nuclear matter at low density [38]. If the parameter B is so large that the antisymmetrization operator \mathcal{A} has no effect, the 3α THSR wave function of Eq. (2.57) actually represents the simple product state where three α particles occupy the same single $0S$ -orbit $\exp(-(2/B^2)X^2)$. On the other hand, in the limit where the parameter B takes its smallest value $B = b$ with b standing for the single-nucleon size parameter of $\phi(\alpha)$ ($v = 1/(2b^2)$), the normalized 3α THSR wave function is equivalent to the shell model wave function;

$$\lim_{B \rightarrow b} N(B) \Phi^{3\alpha\text{THSR}}(B) = |(0s)^4(0p)^8, (0, 4)J = 0\rangle, \quad (2.58)$$

where $N(B)$ is normalization constant. When we calculate the energy curve by the THSR wave function, we have only one energy minimum corresponding to a compact shell-model-like structure and no energy minimum at a large value of B corresponding to the dilute 3α -condensate-like state. Therefore in order to

study the 3α -condensate-like state, we need to perform the GCM calculation by adopting the parameter B as the generator coordinate. In Ref. [37], this GCM calculation with respect to the parameter B was performed for $n\alpha$ systems with $n = 3$ and 4,

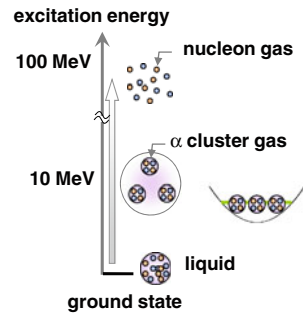
$$\Psi_k(n\alpha) = \sum_j f_j^k \mathcal{A} \left\{ \exp \left[-\frac{2}{B_j^2} \sum_{i=1}^n X_i^2 \right] \phi(\alpha_1) \cdots \phi(\alpha_n) \right\}, \quad (2.59)$$

This GCM calculation gave excited 0^+ state with very large radius in the vicinity of the $n\alpha$ breakup threshold in each $n\alpha$ system ($n = 3$ and 4).

The results of the calculated 0_2^+ state for 3α system were found to be very similar to those of the previous microscopic 3α calculations of Refs. [29–33]. Actually it was soon discovered [39] that the microscopic 3α wave functions of both of Refs. [29–33] have overlaps of more than 95% with a single 3α THSR wave function with a large size parameter B . This result is very striking since the microscopic 3α wave functions of the 0_2^+ state were obtained by solving very complicated integro-differential three-body equation of motion. This striking fact reported in Ref. [39] means without doubt that the Hoyle state structure has a strong relation with the α condensation physics in dilute infinite nuclear matter [38].

The α -particle condensate-like state is the lowest energy state of the α -particle gas-like state. In nuclear physics, gas-like state of nucleons has been an important subject of study for a long time. Such a state has a very high excitation energy and therefore has been a subject of nuclear matter and nuclear reaction rather than nuclear structure. On the other hand, the gas-like state of clusters, if it exists, is not a so highly excited state, and can be a discrete state accessible spectroscopically. This situation is shown in Fig. 2.4. Gas-like state of clusters is a new concept of nuclear structure and this concept was first proposed for the Hoyle state of ^{12}C in 1970s. However, the discussion at that time was confined only for the Hoyle state. Now in 2000s, gas like state of clusters is expected to be universal and is studied in many nuclei both theoretically and experimentally.

Fig. 2.4 Excitation energies of α -cluster gas state and nucleon gas state in the case of ^{12}C



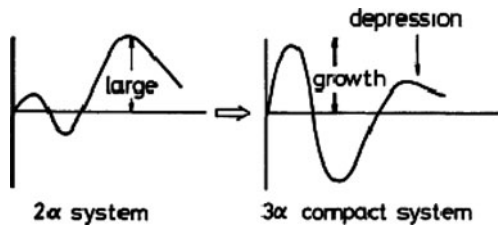
2.3.2.4 Structure Change from the Ground State to the Hoyle State

The energy curve by the 3α THSR wave function shows no local minimum point which corresponds to the Hoyle state and the Hoyle state needs to be obtained by the GCM calculation. When we draw the energy curve by the wave function $(1 - |0_1^+\rangle\langle 0_1^+|)\Phi^{3\alpha\text{THSR}}(B)$ with $|0_1^+\rangle$ standing for the GCM ground state, the energy curve has a minimum point whose wave function is very close to the 0_2^+ state by the GCM calculation [39]. This fact means that the 3α structure of the Hoyle state is largely related to the orthogonality of the Hoyle state to the ground state.

The important role of the orthogonality to the ground state for the formation of the 3α structure of the Hoyle state was discussed already in Ref. [6] from the viewpoint of the 3α dynamics with the α - α interaction described by the OCM. As we explained in the Sect. 2.3.1 on ^8Be , the OCM says that the α - α interaction is composed of two main factors, one is the local attractive potential of the folding-potential type and the other is the orthogonality condition of the α - α relative motion to the Pauli-forbidden states. In the 2α system, because of the orthogonality condition to the Pauli-forbidden states, the relative wave function should have nodes, two nodes for S -wave and one node for D -wave, which means that the relative wave function has the oscillatory behavior in the interaction region. The positions of the nodal points are almost fixed unless we are not treating the high energy motion. The oscillatory behavior of the relative wave function gives rise to a large amount of the kinetic energy. Thus in order to avoid the large kinetic energy, the amplitude of the oscillatory part of the relative wave function becomes small. Small amplitude of the inner part of the relative wave function means that the Pauli-forbidden states act like a repulsive core potential. Actually the radius of the repulsive core of the phenomenological α - α potential like the Ali-Bodmer potential [40] is about 2 fm which is the same as the outermost nodal point.

When the same α - α interaction acts in the 3α system, it is to be noted that the attractive interaction between two α 's becomes effectively stronger than in the 2α system because the attractive interaction via the third α cluster strengthens the α - α attraction in the average by factor 1.5. This point can be explained also in the following way. The 3α Hamiltonian can be written as $H = \sum_i T_i + \sum_{ij} V_{ij} = (2/3) \sum_{ij} [T_{ij} + 1.5V_{ij}]$, where T_{ij} and V_{ij} are the kinetic and interaction operators between i th and j th α clusters. This effectively strengthened α - α attraction drastically changes the inter- α wave function in the interaction region. Namely now the α - α attraction overwhelms the large relative kinetic energy in the inner region, and therefore the amplitude of the relative wave function in the inner region becomes large in order to gain the attractive potential energy. This leads to the formation of the compact ground state of the 3α system (see Fig. 2.5). The formation of the compact ground state affects largely the inter- α relative motion in the excited 0^+ state via the orthogonality of the excited 0^+ state to the compact ground state. The orthogonality to the compact ground state prevents two α 's in the excited 0^+ state from approaching close to each other. This implies the appearance

Fig. 2.5 Change of α - α relative wave function from 2α cluster state to 3α compact state



of the “effective repulsive force” between two α ’s in the excited 0^+ state. Thus in the excited 0^+ state there is a combined repulsive interaction; one is this “effective repulsive force” and the other is the repulsive effect due to the inner oscillation of 2α relative wave function originating from the Pauli-forbidden states. This combined repulsive interaction now overwhelms the strengthened attractive force and expel each α from other α ’s, which explains the formation of the weakly interacting gas-like 3α structure of the Hoyle state. We see thus that the formation of the 3α structure of the Hoyle state is governed by the orthogonality of the Hoyle state to the ground state.

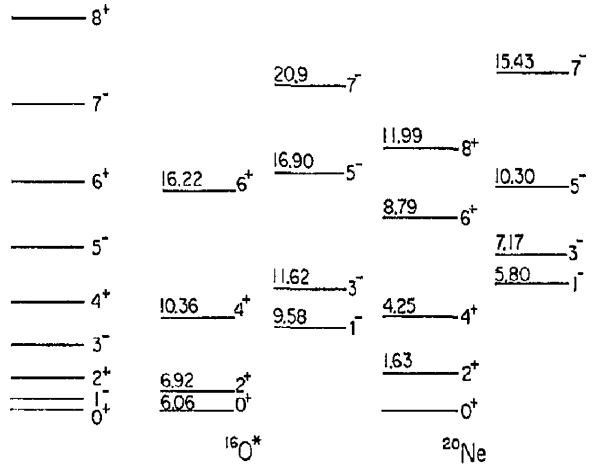
2.3.3 ^{16}O Case

The nucleus ^{16}O is a typical nucleus which shows that nuclear many-body system is rich. It has been long known that, while the ground state is described dominantly by double closed shell wave function, there exist many low-lying excited states which are well described by the $^{12}\text{C} + \alpha$ cluster model around and above the $^{12}\text{C} + \alpha$ threshold. Recently it is strongly suggested that there exist 4α condensate-like states around and above the 4α threshold. The formation of 4α condensate-like states is made by the activation of the α -clustering of the ^{12}C cluster of the $^{12}\text{C} + \alpha$ structure and it is realized by the assistance of the orthogonality to the lower-lying $^{12}\text{C} + \alpha$ states and the ground state.

2.3.3.1 $^{12}\text{C} + \alpha$ Clustering

The ^{16}O nucleus is a doubly magic nucleus and the ground state is described dominantly by double-closed shell structure. Thus this nucleus is a representative nucleus of the nuclear shell model. In spite of this fact, however, the first excited state is located at $E_x = 6.05$ MeV and has spin-parity $J^\pi = 0^+$. Since the value of $\hbar\omega$ in this mass region is about 15 MeV, the positive-parity excitation of the double-closed-shell ground state necessitates excitation energy around $2\hbar\omega \approx 30$ MeV if the mean-field (shell model) dynamics works soundly. Therefore the observed excitation energy 6.05 MeV means that this nucleus is not simply governed by the mean-field dynamics.

Fig. 2.6 Inversion doublet rotational bands in ^{16}O and ^{20}Ne



In 1960s it was experimentally established that this 0_2^+ state is the head state of the positive-parity rotational band with $K^\pi = 0^+$ constituted by $J^\pi = 0^+, 2^+, 4^+, 6^+$ states (Fig. 2.6). In correspondence with this experimental knowledge, an idea of the deformed mean field for this excited rotational band with $K^\pi = 0^+$ prevailed [41, 42]. According to this idea, it is assumed that the ^{16}O nucleus drastically changes its structure from the double closed shell configuration of the ground state into the largely deformed configuration of the $K^\pi = 0_1^+$ rotational band whose dominant component is of four-particle four-hole nature. The small excitation energy of this $K^\pi = 0_1^+$ band was attributed to the small energy gap between the deformed $0p$ -hole orbit and deformed $1s0d$ -particle orbit. Up to now, this interpretation of the 0_2^+ state as having deformed four-particle four-hole structure has remained unchanged in the mean-field model approaches.

Contrary to this deformed four-particle four-hole model which assumes a single common deformed mean field for both particles and holes, the weak coupling model of Ref. [43] considers that particles and holes move in their respective (non-common) mean fields. Namely rotational motion of particles does not couple strongly with that of holes. When the coupling between particles and holes is weak, the 4 $0p$ -holes take the configuration similar to the ground state of ^{12}C and the four $1s0d$ -particles take the configuration similar to the ground rotational band of ^{20}Ne :

$$\Psi(K^\pi = 0_1^+, J) = |(0p)^{-4}(^{12}\text{C}, 0^+), (1s0d)^4(^{20}\text{Ne}, J^+)\rangle. \quad (2.60)$$

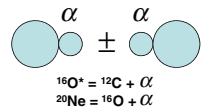
The configuration of four $1s0d$ -particles of ground rotational band states of ^{20}Ne is well approximated by the $\text{SU}(3)$ configuration with the symmetry $(\lambda, \mu) = (8, 0)$. According to the Bayman–Bohr theorem[12], this $\text{SU}(3)$ state is just equivalent to the cluster state with $^{16}\text{O} + \alpha$ structure.

$$|(0s)^4, (0p)^{12}, (1s, 0d)^4; (8, 0)J\rangle = C_{J,\mathcal{A}} \left\{ R_{8,J} \left(r_{O-\alpha}, \frac{16}{5}v \right) Y_J(\hat{r}_{O-\alpha}) \phi(\alpha) \phi(^{16}\text{O}) \right\} \times g(X_G, 20v). \quad (2.61)$$

Thus the weak-coupling model wave function has a relation to the $^{12}\text{C} + \alpha$ cluster wave function.

The $^{12}\text{C} - \alpha$ cluster model gives a very natural explanation of the observed small excitation energy 6.05 MeV of the first excited state (0_2^+) because the threshold energy of $^{12}\text{C} + \alpha$ breakup is located at $E_x = 7.16$ MeV. If this first excited state has a cluster structure of $^{12}\text{C} + \alpha$, the excitation energy 6.06 MeV is very reasonable because it means 1.1 MeV for the binding energy of the $^{12}\text{C} - \alpha$ relative motion. The assignment of $^{12}\text{C} + \alpha$ structure to the first excited state of ^{16}O was suggested already around 1960 by Wildermuth and his coworkers [44, 45]. This work was an underlying knowledge for the weak-coupling model by Arima and his coworkers [43]. The $^{12}\text{C} + \alpha$ cluster structure for the 0_2^+ state with definite idea of spatial localization of clusters was first proposed by Horiuchi and Ikeda [46]. They noticed the negative-parity rotational band states with $J^\pi = 1^-, 3^-, 5^-, 7^-$ (Fig. 2.6) observed by α -particle resonant scattering on ^{12}C by Davis and his coworkers [47–49]. The band head 1^- state is located at $E_x = 9.63$ MeV. The authors of Refs. [47–49] found that the α -widths of the rotational member states are large and comparable with Wigner-limit values and, from these large widths and from the value of the moment of inertia, they interpreted the rotational member states as consisting of an α -cluster rotating outside the ^{12}C core nucleus. The authors of Ref. [46] argued that, if the intrinsic state of this negative-parity rotational band has a $^{12}\text{C} + \alpha$ structure with spatial localization of clusters, the intrinsic state is of parity-asymmetric (parity-violating) shape and hence this intrinsic state should possess a parity-inverted positive-parity rotational band which constitutes a parity doublet (inversion doublet) together with the negative-parity rotational band (Fig. 2.7). They concluded that this positive-parity rotational band is just the observed rotational band upon the 0_2^+ state as the band head state (Fig. 2.6). The main reason for this conclusion was firstly that, as we explained above, there already existed theoretical arguments of Refs. [43–45] which assign the $^{12}\text{C} + \alpha$ structure to this positive parity band upon the 0_2^+ state. The other reason was that there is only this positive-parity band below the negative-parity band of Davis et al. [47–49].

Fig. 2.7 Inversion doublet intrinsic wave functions of core + α clustering



2.3.3.2 $^{12}\text{C} + \alpha$ OCM

In 1970s an extensive study of ^{16}O was performed by Suzuki [50, 51] by using $^{12}\text{C} + \alpha$ coupled-channel OCM [52] where the ^{12}C cluster can be excited to its ground band states with 2^+ and 4^+ . The equation of motion of the coupled-channel OCM for the $^{12}\text{C} + \alpha$ system is given as;

$$(T_i(r) + (\Delta E_C)_i + E_r)\hat{\chi}_i(r) = - \sum_j U_{ij}\hat{\chi}_j(r), \quad \sum_i \langle \chi_i^F(r) | \hat{\chi}_i(r) \rangle = 0, \quad (2.62)$$

$$T_i(r) = \left\langle Y_{\ell_i}(\hat{r}) \left| \frac{-\hbar^2}{2\mu} \frac{\partial^2}{\partial r^2} \right| Y_{\ell_i}(\hat{r}) \right\rangle, \quad (\Delta E_C)_i = E_{L_i}(\text{C}) - E_0(\text{C}), \quad (2.63)$$

$$E_r = E - E(\alpha) - E_0(\text{C}),$$

where μ is the reduced mass of ^{12}C and α and i is the index of a channel with total angular momentum J . $\{\chi_i^F(r)\}$ stand for the Pauli-forbidden states to which $\{\hat{\chi}_i(r)\}$ should be orthogonal. The wave function Ψ^J of the system is obtained from the solution of the relative wave function $\hat{\chi}_i(r)$ as follows,

$$\Psi^J = \mathcal{A} \left[\sum_i \chi_i(r) h_i^J \right], \quad \hat{\chi}_i(r) = \sum_j \int (N_K^{1/2})_{ij}(r, r') \chi_j(r') r'^2 dr', \quad (2.64)$$

$$(N_K)_{ij}(a, b) = \left\langle \frac{\delta(r-a)}{a^2} h_i^J \left| \mathcal{A} \left[\frac{\delta(r-b)}{b^2} h_j^J \right] \right. \right\rangle, \quad h_i^J = [Y_{\ell_i}(\hat{r}) \phi_{L_i}(\text{C})]_J \phi(\alpha). \quad (2.65)$$

The Pauli-forbidden states $\{\chi_i^F(r)\}$ are defined as those states that satisfy

$$\mathcal{A} \left[\sum_i \chi_i^F(r) h_i^J \right] = 0. \quad (2.66)$$

The orthogonality requirement $\sum_i \langle \chi_i^F(r) | \hat{\chi}_i(r) \rangle = 0$ means

$$0 = \sum_i \langle \chi_i^F(r) | \hat{\chi}_i(r) \rangle = \left\langle \sum_i \chi_i^F(r) h_i^J \left| \sum_j \hat{\chi}_j(r) h_j^J \right. \right\rangle. \quad (2.67)$$

The Pauli-forbidden configurations $\sum_i \chi_i^F(r) h_i^J$ are specified by SU(3) irreducible representations and are tabulated in Refs. [50–52].

According to the Bayman–Bohr theorem [12], the double closed shell wave function of ^{16}O can be described with the cluster model wave function:

$$\begin{aligned} \det |(0s)^4(0p)^{12}| &= c_L \mathcal{A} \left[R_{4,L}(r_{\text{C}-\alpha}, 3v) \left[Y_L(\hat{r}_{\text{C}-\alpha}) \phi_L(^{12}\text{C}) \right]_{J=0} \phi(\alpha) \right] \\ &\times g(X_G, 16v), \end{aligned} \quad (2.68)$$

where $R_{4,L}(r, 3\nu)$ is harmonic oscillator radial function with oscillator parameter 3ν , angular momentum L and number of oscillator quanta 4, $4 = 2n + L$. This equality holds for any L among $L = 0, 2$, and 4. Thus this OCM study could treat the ground state and accordingly the structure change between the shell-model-like structure and the cluster structure. The calculated results were very successful in reproducing almost all the observed data. The good reproduction of the energy spectra is shown in Fig. 2.8. Table 2.5 shows the good reproduction of electric transition data. The ground state was shown to be dominantly given by double closed shell wave function and the $K^\pi = 0_1^+$ and $K^\pi = 0_1^-$ bands were shown to have dominantly the $^{12}\text{C}(0_1^+) + \alpha$ cluster structure. Furthermore the negative parity states with $3_1^-, 1_1^-, 2_1^-$ were shown to have dominantly shell model structure with 1-particle 1-hole excitation although rather large mixture of cluster configuration is existent. Beside the good reproduction of energy spectra and electric transitions shown in Fig. 2.8 and Table 2.5, alpha-decay data are also well reproduced as shown in Table 2.6. The $^{12}\text{C}(2_1^+) + \alpha$ structure with S -wave of α motion is realized in the observed 2_2^+ state at 9.85 MeV.

The results of the $^{12}\text{C} + \alpha$ OCM deny the formation of single deformed structure composed of strong coupling of the rotational motion of ^{12}C cluster and the orbiting motion of α cluster around ^{12}C cluster. In the case of the 2_2^+ state at 9.85 MeV, as mentioned above, the dominant component of the 2_2^+ wave function is composed of $^{12}\text{C}(2^+)$ coupled with S -wave α cluster. This result is in

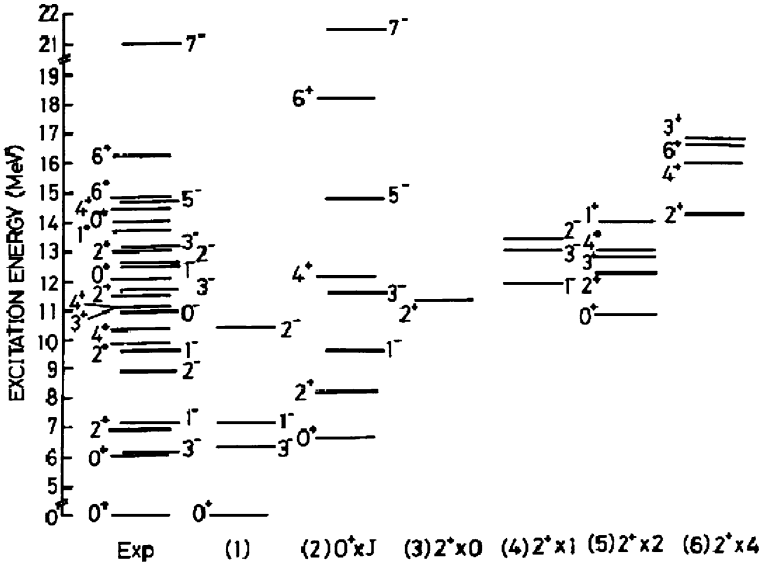


Fig. 2.8 Energy spectra by $^{12}\text{C} + \alpha$ OCM [6, 50, 51] classified by dominant component $L^+ \times \ell(^{12}\text{C}(L^+) + \alpha(\ell))$. Classification denoted as (1) is for the mean-field-type states including the ground state and 1p - 1h type states

Table 2.5 Electric transition rates in ^{16}O compared with $^{12}\text{C} + \alpha$ OCM calculation [50, 51]

Transition	exp.	$^{12}\text{C} + \alpha$
$B(E2)(e^2\text{fm}^4)$		
$2_1^+ \rightarrow 0_1^+$	7.8 ± 0.3	2.20
$2_1^+ \rightarrow 0_2^+$	76 ± 13	60.2
$1_1^- \rightarrow 3_1^-$	51 ± 10	25.5
$2_1^- \rightarrow 3_1^-$	14_{-4}^{+3}	13.8
$2_1^- \rightarrow 1_1^-$	36 ± 5	15.1
$2_2^+ \rightarrow 0_1^+$	0.082 ± 0.007	0.247
$2_2^+ \rightarrow 0_2^+$	3.0 ± 0.7	9.68
$4_1^+ \rightarrow 2_1^+$	150 ± 18	102
$4_2^+ \rightarrow 2_1^+$	2.4 ± 0.6	0.0405
$2_3^+ \rightarrow 0_1^+$	3.7 ± 0.1	1.21
$2_3^+ \rightarrow 0_2^+$	7.6 ± 2	1.20
$M(E0)(\text{fm}^2)$		
$0_1^+ - 0_2^+$	3.55 ± 0.21	3.88
$0_1^+ - 0_3^+$	4.03 ± 0.09	3.50
$B(E3)(e^2\text{fm}^6)$		
$3_1^- \rightarrow 0_1^+$	213 ± 11	130

accordance with the weak-coupling shell model of Ref. [43] which describes this 2_2^+ state as composed of the four-hole configuration $(0p)^{-4}(J_h = 2)$ and the four-particle configuration $(1s0d)^4(J_p = 0)$. In usual mean-field models, this state is

Table 2.6 Alpha decay data in ^{16}O compared with $^{12}\text{C} + \alpha$ OCM calculation [50, 51]

J^π (Ex (MeV))	Γ (keV)	Decay	θ_{exp}^2	θ_{cal}^2
1_2^- (9.63)	510 ± 60	α_0	0.71	0.59
2_2^+ (9.85)	0.9 ± 0.3	α_0	0.0019	0.0079
4_1^+ (10.35)	27 ± 4	α_0	0.37	0.42
4_2^+ (11.10)	0.28 ± 0.05	α_0	0.0011	0.047
2_3^+ (11.52)	74 ± 4	α_0	0.033	0.048
3_2^- (11.60)	800 ± 100	α_0	0.63	0.51
0_3^+ (12.05)	1.5 ± 0.5	α_0	0.00037	0.097
1_3^- (12.44)	98 ± 7	α_0	0.024	0.000064
	0.025	α_1	0.084	0.18
2_2^- (12.53)	≤ 0.5	α_1	≤ 0.59	0.13
2_4^+ (13.02)	150 ± 11	α_0	0.039	0.069
3_3^- (13.13)	90 ± 14	α_0	0.032	0.091
	≈ 20	α_1	≈ 0.36	0.41
1_1^+ (13.66)	64 ± 3	α_1	0.54	0.54
5_1^- (14.67)	530 ± 71	α_0	0.38	0.30
	28 ± 4	α_1	0.10	0.074
6_1^+ (14.82)	22	α_0	0.043	0.025
	48	α_1	0.62	0.41
6_2^+ (16.29)	490 ± 40	α_0	0.42	0.42
7_2^- (20.88)	650 ± 75	α_0	0.27	0.34

Reduced widths θ^2 are at the channel radius $a = 5.2$ fm

regarded as the band-head state of the $K^\pi = 2^+$ side band with four-particle four-hole structure.

2.3.3.3 4α OCM and 4α -Gas Like States

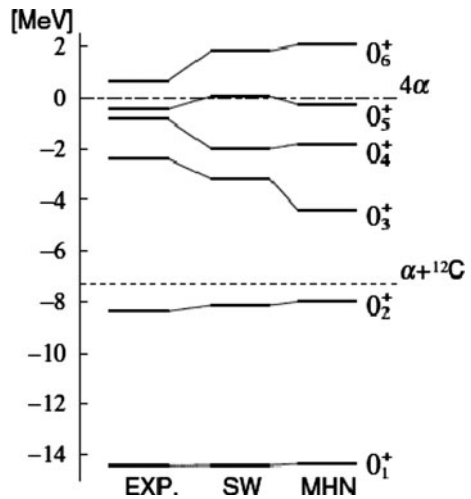
Recently Funaki and his coworkers have reported the results of the full four-body calculations in the framework of 4α OCM [53]. They claim that the calculated lowest six 0^+ states reproduce or well correspond to the observed six 0^+ states up to the 0_6^+ state at 15.1 MeV as shown in Fig. 2.9. The calculated 0_1^+ has, as its dominant component, the double closed shell wave function. From the calculation of the reduced width amplitudes $y(r)$ of various $^{12}\text{C} + \alpha$ channels,

$$y(r) = \left\langle \frac{\delta(r_{C-\alpha} - r)}{r^2} \left[Y_L(\hat{r}_{C-\alpha}) \phi_L(^{12}\text{C}) \right]_0 \middle| \Phi(^{16}\text{O}, 0_k^+) \right\rangle, \quad (2.69)$$

the calculated 0_2^+ and 0_3^+ states proved to have, as their dominant components, $^{12}\text{C}(0_1^+) + \alpha$ and $^{12}\text{C}(2_1^+) + \alpha$ cluster structures, respectively. In Eq. (2.69) $\phi_L(^{12}\text{C})$ is the wave function of ^{12}C given by the 3α OCM calculation [54] with the same effective inter- α interaction. One of the most important results of Ref. [53] is that the calculated 0_6^+ state has a structure of 4α -condensate-like state. The radius of the calculated 0_6^+ state has a very large value of about 5 fm. This large size suggests that the calculated 0_6^+ state is composed of a weakly interacting gas of α particles. The reduced width amplitudes $y(r)$ of the calculated 0_6^+ state proved to have a large amplitude only in the $^{12}\text{C}(0_2^+) + \alpha$ channel.

From the analyses of the reduced width amplitudes in various $^{12}\text{C} + \alpha$ channels, the calculated 0_4^+ and 0_5^+ states were found to have dominantly $^{12}\text{C}(0_1^+) + \alpha$ and

Fig. 2.9 Energy spectra by 4α OCM [53] with two kinds of effective nuclear force, SW and MHN



$^{12}\text{C}(1^-) + \alpha$ cluster structures, respectively. The widths of the calculated $0_4^+, 0_5^+$ and 0_6^+ states are ~ 150 , ~ 50 , and ~ 50 keV, respectively, while those of the observed $0_4^+, 0_5^+$ and 0_6^+ states are 600, 185, and 166 keV, respectively.

The full four-body calculation of alpha clusters of Ref. [53] shows us that nuclear many-body system undergoes actually drastic structure changes as the excitation energy increases, namely from compact shell-model-like structure to various $^{12}\text{C} + \alpha$ structures and furthermore to a 4α gas-like structure. Since the various $^{12}\text{C} + \alpha$ structures have been well confirmed to be realized in many excited states, the calculations of Ref. [53] which succeeded to reproduce these $^{12}\text{C} + \alpha$ states can be regarded as highly reliable.

2.3.4 ^{20}Ne Case

2.3.4.1 Ikeda Diagram and Transitional Character of the Ground Band Between Mean-Field Like Structure and Cluster Structure

As we mentioned in the previous section on ^{16}O , Horiuchi and Ikeda proposed in ^{16}O to regard the $K^\pi = 0^+$ band upon 6.05 MeV 0^+ state and $K^\pi = 0^-$ band upon 9.63 MeV 1^- state as being inversion doublet bands with the parity-violating structure of $^{12}\text{C} + \alpha$ [46]. In the same Ref. [46] the authors also proposed in ^{20}Ne to regard the $K^\pi = 0^+$ ground band and $K^\pi = 0^-$ band upon 5.78 MeV 1^- state as being inversion doublet bands with the parity-violating structure of $^{16}\text{O} + \alpha$ (Figs. 2.7, 2.8). One of the grounds of this proposal was the report given in Ref. [47–49] which reported on the resonant scattering of α particles on ^{16}O together with that on ^{12}C . The authors of Refs. [47–49] found that the α -widths of the $K^\pi = 0^-$ band member states are large to be comparable with Wigner-limit values and, from these large widths and from the value of the moment of inertia, they interpreted the $K^\pi = 0^-$ band member states as having a structure of $^{16}\text{O} + \alpha$. Another ground of the proposal was the fact that the shell model study of the ^{20}Ne teaches us that the dominant component of the ground band is given by the SU(3) configuration with $(\lambda, \mu) = (8, 0)$, $|(0s)^4, (0p)^{12}, (1s, 0d)^4; (8, 0)J\rangle$ [55, 56]. According to the Bayman–Bohr theorem this wave function is equivalent to the $^{16}\text{O} + \alpha$ cluster model wave function as was shown in Eq. (2.61). It was also important to note that below the $K^\pi = 0^-$ band upon 5.78 MeV 1^- state the ground band is the only band with $K^\pi = 0^+$.

Ikeda and his collaborators noticed the fact that the states in light nuclei which were assigned to have cluster structures are energetically located near or above the cluster-breakup thresholds corresponding to respective cluster structure. Typical examples are ground band states of ^8Be , the Hoyle state of ^{12}C , and the above-explained inversion doublet band states in ^{16}O and in ^{20}Ne . Supported by this fact, they proposed the so-called Ikeda diagram which gives necessary conditions for the formation of cluster states [57] (Fig. 2.10). The first condition is the stability of

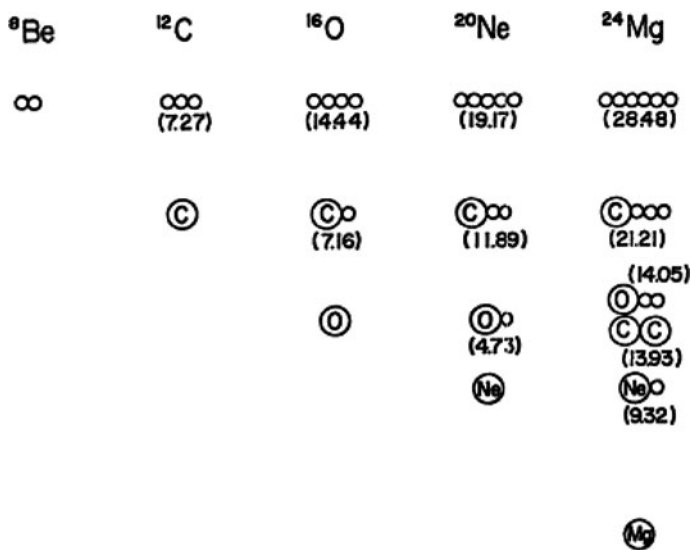


Fig. 2.10 Ikeda diagram [57]

the constituent clusters which is necessary for keeping the identity of the clusters. The second condition is the weakness of inter-cluster interaction. If the inter-cluster interaction is strongly attractive, the clusters will dissolve into mean-field-like structure. The weakness of the inter-cluster interaction results in the energy location of the cluster state near the breakup threshold into constituent clusters. Thus the Ikeda diagram says that the energy location of the cluster state is necessarily near the breakup threshold into constituent clusters. Usually ground states of nuclei are located well below the α breakup threshold and thus they have mean-field-like structure. A clear violation for this statement is the ground state of ^8Be which is located slightly above the α - α breakup threshold. The well-known fact that the ground state of ^8Be has an α - α cluster structure is in good accordance of the Ikeda diagram.

As mentioned above, the ground state is usually considered to have mean-field-like structure except the case of ^8Be . But in Ref. [46] the authors assigned the $^{16}\text{O} + \alpha$ cluster structure to the ground state of ^{20}Ne . Thus this assignment needs to be checked carefully. The ground state of ^{20}Ne is located below the $^{16}\text{O} + \alpha$ breakup threshold by 4.73 MeV. This value of 4.73 MeV is fairly smaller than the corresponding binding energies of the ground states measured from the α breakup threshold in other nuclei. For example in ^{12}C the ground state is located below the $^8\text{Be} + \alpha$ or 3α threshold by about 7.5 MeV and also in ^{16}O the ground state is located below the $^{12}\text{C} + \alpha$ threshold also by about 7.2 MeV. Hence it is conceivable that the ground state of ^{20}Ne does not have so good cluster structure of $^{16}\text{O} + \alpha$. At the same time it is conceivable that the ground state of ^{20}Ne does not have so good mean-field-like structure. This intermediate character of the ground band of ^{20}Ne was noticed from the beginning in Refs. [46, 57] and was

named [58, 6] “transitional character of the ground band of ^{20}Ne between mean-field like structure and cluster structure”. In Refs. [46, 57] it was pointed out that, because of the transitional character of ^{20}Ne ground band, the magnitude of the gap energy between the band head states of the $K^\pi = 0^+$ band and the $K^\pi = 0^-$ band is much larger in ^{20}Ne (5.5 MeV) than in ^{16}O (3.0 MeV).

2.3.4.2 AMD Study of ^{20}Ne

AMD studies of ^{20}Ne [59–61] have made important contributions for the clarification of structural problems of ^{20}Ne , including the transitional character of the ground band. Figure 2.11 shows good reproduction of the observed energy spectra by the calculation of Ref. [60]. Table 2.7 shows that the $E2$ transitions inside the ground, $K^\pi = 0_1^-$, and $K^\pi = 2_1^-$ bands are also well reproduced by the calculation of Ref. [60] without use of any effective charge. The magnitudes of the deformations of the $K^\pi = 0_1^+$ (ground), $K^\pi = 0_1^-$, and $K^\pi = 2_1^-$ bands are shown in their energy curves with respect to the quadrupole deformation parameter β in Fig. 2.12. Here “deformed-basis AMD” means that the nucleon wave packets of AMD wave function are deformable while “spherical-basis AMD” means that the nucleon wave packets of AMD wave function are kept spherical. We note that for the $K^\pi = 0_1^+$ and $K^\pi = 2_1^-$ bands the deformation of nucleon wave packets makes the binding energies of these bands appreciably deeper while for the $K^\pi = 0_1^-$ band the nucleon wave packets favor spherical shape. The value of β at the minimum energy point is about 0.4 for both the $K^\pi = 0_1^+$ and $K^\pi = 2_1^-$ bands while it is about 0.5 for the $K^\pi = 0_1^-$ band. The $^{16}\text{O} + \alpha$ clustering features of these three bands can be seen in Fig. 2.13 which shows the position of centroids of the nucleon wave packets of the AMD wave function. This figure shows that

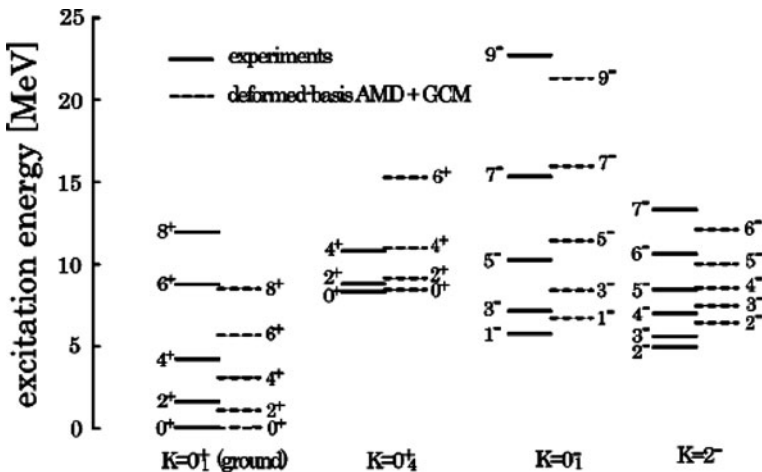
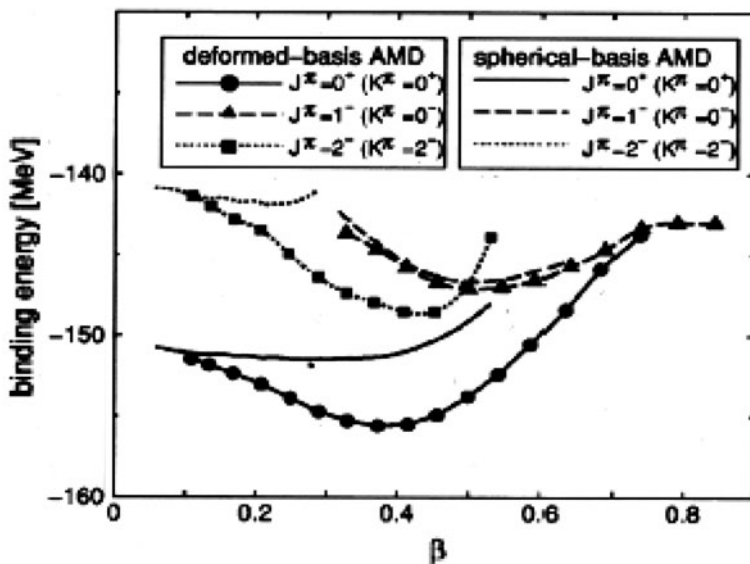


Fig. 2.11 Energy spectra of ^{20}Ne by AMD [60]

Table 2.7 $B(E2)$ ($e^2\text{fm}^2$) in ^{20}Ne compared with AMD calculation [60]

$J_i^\pi \rightarrow J_f^\pi$	EXP	AMD
$[K^\pi = 0_1^+]$		
$2_1^+ \rightarrow 0_1^+$	65 ± 3	70.3
$4_1^+ \rightarrow 2_1^+$	71 ± 6	83.7
$6_1^+ \rightarrow 4_1^+$	64 ± 10	52.7
$8_1^+ \rightarrow 6_1^+$	29 ± 4	21.0
$[K^\pi = 0^-]$		
$3^- \rightarrow 1^-$	164 ± 26	151.2
$[K^\pi = 2^-]$		
$3_1^- \rightarrow 2^-$	113 ± 29	102.8
$4^- \rightarrow 3_1^-$	77 ± 16	77.8
$4^- \rightarrow 2^-$	34 ± 6	38.5
$5_1^- \rightarrow 4^-$	<808	84.5
$5_1^- \rightarrow 3_1^-$	84 ± 19	56.6
$6_1^- \rightarrow 5_1^-$	32 ± 13	29.9
$6^- \rightarrow 4^-$	55^{+23}_{-13}	64.0

**Fig. 2.12** Energy curves of ^{20}Ne with respect to quadrupole deformation by AMD [60]

the $K^\pi = 0_1^-$ wave function around $\beta = 0.5$ has nucleon wave packets of an α cluster separated largely apart from other 16 nucleon wave packets. This means that the $K^\pi = 0_1^-$ band has a clear cluster structure of $^{16}\text{O} + \alpha$. On the contrary, the nucleon wave packets of the $K^\pi = 2_1^-$ wave function around $\beta = 0.4$ are all located close to one another. This means that the $K^\pi = 2_1^-$ band has a mean-field-type structure. The wave function of the $K^\pi = 0_1^+$ band at the minimum energy

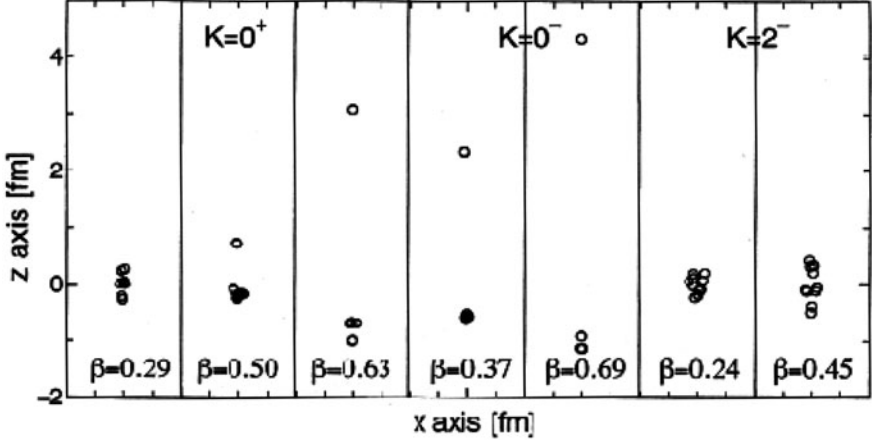


Fig. 2.13 Spatial positions of nucleon-wave-packet centroids of AMD wave functions of ^{20}Ne [60]

point around $\beta = 0.4$ is seen to have rather similar spatial distribution of nucleon wave packets to that of the $K^\pi = 2^-$ band. However it is also seen that the $K^\pi = 0^+$ band wave function with slightly larger $\beta = 0.5$ has a feature of weak clustering of $^{16}\text{O} + \alpha$. Fig. 2.14 gives the density distributions of the intrinsic wave functions which have nucleon wave packet distributions shown in Fig. 2.13. We see in this figure that the density distribution of the $K^\pi = 0^-$ intrinsic state around $\beta = 0.5$ has a clear parity-violating shape due to the $^{16}\text{O} + \alpha$ clustering while that of the $K^\pi = 0^+$ intrinsic state in the region of $\beta = 0.3 \sim 0.5$ does not show, just like the $K^\pi = 2^-$ band with mean-field-type structure, clear parity-violating shape.

Although the density distribution of the intrinsic state of the ground band does not have a clear parity-violating shape due to the $^{16}\text{O} + \alpha$ clustering, the wave function of the ground band has a large component of $^{16}\text{O} + \alpha$ clustering. Table 2.8 shows that the squared amplitude of the $^{16}\text{O} + \alpha$ component W^J of the ground band is about 70% for low spin states and decreases to about 30% for high spin states. The magnitude W^J of the $^{16}\text{O} + \alpha$ component of a given wave function Φ^J is obtained as $W^J = |\alpha_J|^2$ with α_J defined as

$$\Phi^J = \alpha_J \Phi^J(^{16}\text{O} + \alpha) + \sqrt{1 - |\alpha_J|^2} \Phi_R^J, \quad (2.70)$$

$$\Phi^J(^{16}\text{O} + \alpha) = n_J \mathcal{A} \left\{ \chi_J(r_{\text{O}-\alpha}) Y_J(\hat{r}_{\text{O}-\alpha}) \phi(^{16}\text{O}) \phi(\alpha) \right\}, \quad (2.71)$$

where $\Phi^J(^{16}\text{O} + \alpha)$ is normalized wave function in the functional space of $^{16}\text{O} + \alpha$ and Φ_R^J is normalized component orthogonal to the $^{16}\text{O} + \alpha$ functional space. A detailed explanation how to calculate W^J is given in Sect. 2.3.4.3. For the large value of $W^J = 70\%$, the fact due to the Bayman–Bohr theorem given in Eq. (2.61), $|(0s)^4, (0p)^{12}, (1s, 0d)^4; (8, 0)J\rangle = C_J \mathcal{A} \{ R_{8,J}(r_{\text{O}-\alpha}, (16/5)v) Y_J(\hat{r}_{\text{O}-\alpha})$

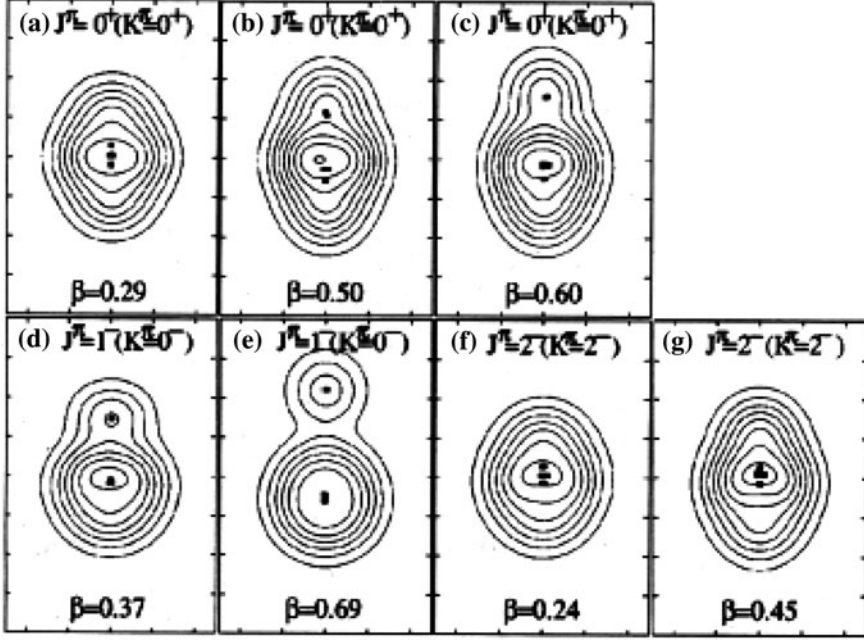


Fig. 2.14 Density distributions of AMD intrinsic wave functions with various quadrupole deformation [60]

$\phi(\alpha)\phi(^{16}\text{O})\}g(X_G, 20\nu)$, makes a large contribution. The percentage of the $^{16}\text{O} + \alpha$ component of the $K^\pi = 0_1^-$ band is much larger than the ground band and is about 95% for low spin states but it again decreases to about 70% for high spin states. We can regard that the magnitude of $W^J = 70\%$ for the ground band is large enough to allow the inversion doublet picture for the ground band and $K^\pi = 0_1^-$ band.

AMD calculation reproduces the $K^\pi = 0_4^+$ band which has the band head 0^+ state at 8.3 MeV. This band has been known by many cluster model studies [6] to have an $^{16}\text{O} + \alpha$ structure which has one more nodal points in their relative wave functions of $^{16}\text{O} - \alpha$ compared with the ground band. In terms of the quantum number $N = 2n + L$ with n standing for the number of nodes, the $K^\pi = 0_4^+$ band has $N = 10$, while for the ground and $K^\pi = 0_1^-$ bands $N = 8$ and 9, respectively. Table 2.8 shows the magnitude of W^J of the $K^\pi = 0_4^+$ band is about 80% for low spin states and it decreases to about 60% for high spin states. The $^{16}\text{O} + \alpha$ clustering character is reflected in the α decay strength. Table 2.9 shows that the observed α decay strengths of the ground, $K^\pi = 0_1^-$, and $K^\pi = 0_4^+$ bands are well reproduced by the AMD calculations.

In all three bands of $K^\pi = 0_1^+$, $K^\pi = 0_1^-$, and $K^\pi = 0_4^+$, the magnitude W^J of the $^{16}\text{O} + \alpha$ component decreases from low spin to high spin states. An important reason of this decrease is the nucleon spin alignment which is against the formation of α cluster [59]. Figure 2.15 shows the expectation value of the intrinsic spin

Table 2.8 Squared amplitudes of $^{16}\text{O} + \alpha$ component W^J and expectation values of two-body spin-orbit force $\langle \bar{V}_{ls} \rangle$ by AMD [60]

K^π	J^π	W^J	$\langle \bar{V}_{ls} \rangle$
0_1^+	0_1^+	0.70	-5.2
	2_1^+	0.68	-5.3
	4_1^+	0.54	-5.9
	6_1^+	0.34	-8.4
	8_1^+	0.28	-10.9
0_4^+	0_4^+	0.82	-3.2
	2_4^+	0.81	-3.0
	4_4^+	0.79	-4.9
	6_4^+	0.67	-6.8
	8_4^+	0.55	-7.4
0_1^-	1_1^-	0.95	-0.8
	3_2^-	0.93	-0.8
	5_2^-	0.88	-0.7
	7_2^-	0.71	-0.9
	9_2^-	0.70	-1.3
2^-	2_1^-		-12.9
	3_1^-		-13.0
	4_1^-		-14.1
	5_1^-		-14.4
	6_1^-		-16.5

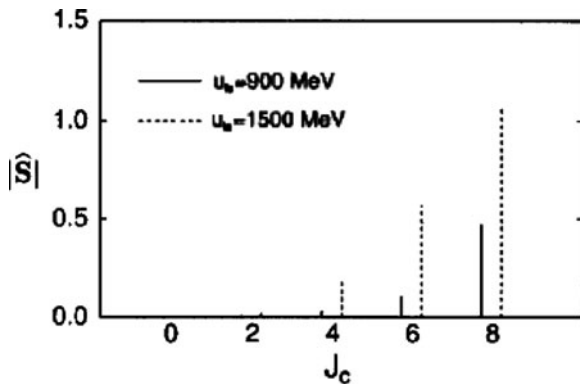
Table 2.9 α reduced widths θ^2 multiplied by 100 in ^{20}Ne compared with AMD calculations [60]

K^π	J^π	EXP	AMD
0_1^+	6_1^+	1.0 ± 0.2	0.53
	8_1^+	0.094 ± 0.027	0.08
0_4^+	0_4^+	>50	69.0
	2_4^+	>59	68.0
	4_4^+	23	35.5
0_1^-	1^-	>16	31.0
	3_2^-	26	29.1
	5_2^-	30	28.8
	7_2^-	22 ± 5	11.5
	9^-	17	8.9

Channel radius a is 6 fm

angular momentum (non orbital angular momentum) in the ground band which grows larger for high spin states. The nucleon spin alignment is reflected in the expectation value of the two-body spin-orbit force which, for the ground band, is -5.2 MeV for the $J^\pi = 0_1^+$ state and increases to -8.4 MeV for the $J^\pi = 8_1^+$ state. Since the $K^\pi = 0_1^-$ band has very large component of $^{16}\text{O} + \alpha$, the expectation value of the two-body spin-orbit force is small and is only -0.8 MeV for the $J^\pi = 1^-$ state, but it still increases to -1.3 MeV the $J^\pi = 9^-$ state. The effect of the nucleon spin alignment is reflected in the shape of the quadrupole

Fig. 2.15 Expectation values of intrinsic spin angular momentum for the ground band states of ^{20}Ne by AMD [59]



deformation [60]. Figure 2.16 shows that the ground band intrinsic wave function of AMD changes its shape from prolate deformation for low spin states to the oblate deformation of the $J^\pi = 8^+$ state. This effect was discussed in detail in Ref. [59]. It is quite interesting that the nucleon spin alignment which is a mean-field-like dynamics is coexistent together with the clustering dynamics in the ground band and also even in the typical cluster band of $K^\pi = 0_1^-$.

In this lecture we do not discuss the $K^\pi = 0_2^+$ and $K^\pi = 0_3^+$ bands whose band-head $J^\pi = 0^+$ states are located between the ground state and the $K^\pi = 0_4^+$

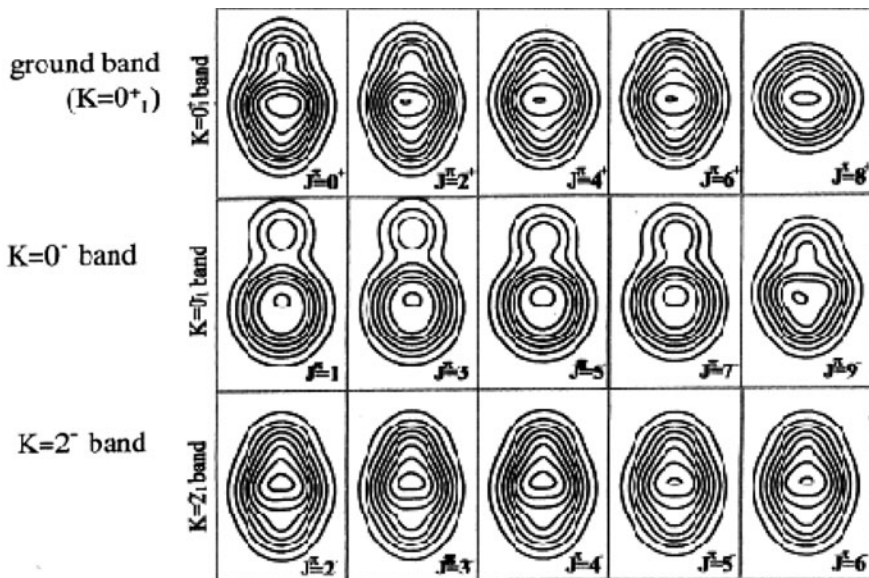


Fig. 2.16 Change of deformation with increase of angular momentum for ground, $K^\pi = 0^-$, and $K^\pi = 2^-$ bands of ^{20}Ne [60]

band-head $J^\pi = 0^+$ state. The $K^\pi = 0_2^+$ band has a shell-model-like structure with less collectivity than the ground band [6]. The $K^\pi = 0_3^+$ band has been discussed to have a $^{12}\text{C} + 2\alpha$ structure [6] which has been recently supported by an AMD calculation [61].

2.3.4.3 Projection Operator onto the Cluster Model Space

The projection operator onto the cluster model space can be constructed by using the eigenvalues and eigenfunctions of the RGM norm kernel N_K [63]. Here we explain a practical method of numerical construction of the projection operator onto the cluster model space spanned by the wave functions of the form $\mathcal{A}\{\chi_L(r)Y_L(\hat{r})\phi(C_1)\phi(C_2)\}$ with r standing for the relative coordinate between clusters C_1 and C_2 . We first prepare sufficient number of Brink wave functions $\{\Psi_L(R_i), (i = 1 \sim N)\}$,

$$\Psi_L(R) = D(R)P_L\mathcal{A}\{\psi(C_1, n_1 r)\psi(C_2, n_2 r)\} = \Phi_L(R)g(X_G, Av), \quad (2.72)$$

$$\Phi_L(R) = D(R)P_L\mathcal{A}\{g(r - r, A_r v)\phi(C_1)\phi(C_2)\} \quad (2.73)$$

$$n_1 = \frac{A_2}{A}, \quad n_2 = -\frac{A_1}{A}, \quad A_r = \frac{A_1 A_2}{A}, \quad A = A_1 + A_2, \quad (2.74)$$

where P_L is the projection operator of angular momentum, $D(R)$ is normalization constant, and A_1 and A_2 are mass numbers of the clusters C_1 and C_2 , respectively. The functional space spanned by $\{\Phi_L(R_i), (i = 1 \sim N)\}$ is intended to be approximately the same as the cluster model space under consideration. The orthonormal basis wave functions $\{\hat{\Phi}_L^i, (i = 1 \sim N)\}$ of this functional space are obtained by diagonalizing the overlap matrix $\{A_{ij}\}$ with orthogonal matrix $\{e_{ij}\}$,

$$\hat{\Phi}_L^i = \frac{1}{\sqrt{\mu_i}} \sum_{j=1}^N e_{ij} \Phi_L(R_j), \quad \sum_{i=1}^N A_{ij} e_{kj} = \mu_k e_{ki}, \quad (2.75)$$

$$A_{ij} = \langle \Phi_L(R_i) | \Phi_L(R_j) \rangle = \langle \Psi_L(R_i) | \Psi_L(R_j) \rangle. \quad (2.76)$$

The desired projection operator P onto the cluster model space and the percentage W^J of the $C_1 + C_2$ cluster component of a given wave function Φ are approximately calculated as

$$P = \sum_{i=1}^N |\hat{\Phi}_L^i\rangle \langle \hat{\Phi}_L^i| = \sum_{i,j=1}^N (A^{-1})_{ij} |\Phi_L^i\rangle \langle \Phi_L^j|, \quad (2.77)$$

$$W^J = \langle \Phi | P | \Phi \rangle = \sum_{i,j=1}^N (A^{-1})_{ij} \langle \Phi | \Phi_L^i \rangle \langle \Phi_L^j | \Phi \rangle. \quad (2.78)$$

2.4 Coexistence of Cluster Structure and Superdeformation in Heavy *sd*-Shell and Light *pf*-Shell Nuclei

Studies of cluster states in heavy *sd*-shell and light *pf*-shell nuclei have been pursued by many authors but microscopic studies have not been so extensive as in light *sd*-shell and *p*-shell nuclei. One of the characteristic features of the studies of clustering in this mass number region is the study of molecular resonances in somewhat high excitation energy region [64–66]. Recently a new stimulation has been brought to this subject by the accumulation of the experimental knowledge of superdeformed and hyperdeformed states in this mass number region which is by the use of powerful gamma detectors used in heavier mass regions. Representative examples are for nuclei like ^{36}Ar [67], ^{38}Ar [68], ^{40}Ca [69], and ^{44}Ti [70]. For the study of the coexistence of cluster states and mean-field-type states, the study of the interrelation between superdeformed states and cluster states including molecular resonances is a very important new subject to be investigated more in future. In this lecture we discuss this subject in two nuclei, ^{44}Ti and ^{32}S .

2.4.1 ^{44}Ti Case

2.4.1.1 $^{40}\text{Ca} + \alpha$ Cluster States and Superdeformed States

The ^{44}Ti nucleus is the *pf*-shell analogue of the nucleus ^{20}Ne and several studies by using microscopic $^{40}\text{Ca} + \alpha$ cluster wave function were performed [71–73]. An important knowledge on the $^{40}\text{Ca} + \alpha$ structure in ^{44}Ti was obtained by using the unique $^{40}\text{Ca} + \alpha$ potential which was derived by fitting the anomalous large angle scattering (ALAS) and nuclear rainbow phenomena of $^{40}\text{Ca} + \alpha$ elastic scattering [66, 74]. The lowest 0^+ state of this potential was found to be located about 4 MeV below the $^{40}\text{Ca} + \alpha$ threshold which is near the experimental ground state located about 5 MeV below the threshold ($E_{th} = 5.14$ MeV). This result suggested that the ground state contains large component of $^{40}\text{Ca} + \alpha$ cluster structure [75–77]. Similar conclusion was obtained by the $^{40}\text{Ca} + \alpha$ RGM study of Ref. [78]. In this RGM study the parameters of the effective nuclear force were chosen so as to reproduce the observed elastic scattering cross sections in a wide energy range by using the same imaginary potential as Ref. [74]. Then this RGM calculation proved to give the lowest 0^+ state near the experimental ground state.

An important experimental finding which supports the existence of the $^{40}\text{Ca} + \alpha$ cluster structure in ^{44}Ti was obtained by the α transfer experiment on ^{40}Ca [80]. This transfer experiment confirmed the existence of the negative-parity rotational band with $K^\pi = 0^-$ which has the $^{40}\text{Ca} + \alpha$ cluster structure. The band head 1^- level was found at ~ 7 MeV and band member states were found to have large α spectroscopic factors. As are the cases of the $^{12}\text{C} + \alpha$ structure in ^{16}O and the $^{16}\text{O} + \alpha$ structure in ^{20}Ne , the existence of the negative-parity rotational band with

$K^\pi = 0^-$ is a necessary condition in order for the $^{40}\text{Ca} + \alpha$ cluster structure to exist.

The two low-lying rotational bands, one with $K^\pi = 0_2^+$ upon 0_2^+ state at 1.90 MeV and the other with $K^\pi = 2^+$ upon 2^+ state at 2.89 MeV, are now suggested to be a superdeformed band and its side band, respectively [70]. The low spin members of these bands have been known since long [81, 82] and recently their high spin members were found to extend up to $J^\pi = 12^+$ states. Shell model calculation assigned 8-particle four-hole configuration to this superdeformed band [83], and mean-field-type calculations confirmed the appearance of low-lying 8-particle four-hole band [84, 85] with superdeformation. On the other hand some cluster model studies assume $^{40}\text{Ca}^* + \alpha$ cluster structure to this band [77, 86, 87] with $^{40}\text{Ca}^*$ standing for the 0_2^+ and 2_1^+ states assumed to have $^{36}\text{Ar} + \alpha$ cluster structure.

2.4.1.2 AMD Study of ^{44}Ti

AMD study of ^{44}Ti in Ref. [8] has contributed for the clarification of the actual coexistence features of $^{40}\text{Ca} + \alpha$ cluster states and mean-field-type states including superdeformed states.

Figure 2.17 shows good reproduction of the observed energy spectra by the calculation of Ref. [88]. Table 2.10 shows that the $E2$ transitions, intra-band transitions inside the ground band and two superdeformed bands with $K^\pi = 0_2^+$ and $K^\pi = 2^+$ and also the inter-band transitions between $K^\pi = 0_2^+$ and $K^\pi = 2^+$ bands, are well reproduced by the calculation of Ref. [88] without use of any effective charge.

Table 2.10 $B(E2)$ ($e^2\text{fm}^2$) in ^{44}Ti compared with AMD calculation [88]

$J_i^\pi \rightarrow J_f^\pi$	EXP	AMD
$[K^\pi = 0_1^+]$		
$2_1^+ \rightarrow 0_1^+$	120 ± 30	142
$4_1^+ \rightarrow 2_1^+$	280 ± 60	222
$6_1^+ \rightarrow 4_1^+$	160 ± 30	167
$8_1^+ \rightarrow 6_1^+$	$14 >$	172
$10_1^+ \rightarrow 8_1^+$	140 ± 30	99
$12_1^+ \rightarrow 10_1^+$	40 ± 8	69
$[K^\pi = 2^+ \rightarrow K^\pi = 0_2^+]$		
$2_3^+ \rightarrow 0_2^+$	$43 <$	24
$[K^\pi = 0_2^+]$		
$2_2^+ \rightarrow 0_2^+$	220 ± 50	320
$4_2^+ \rightarrow 2_2^+$	268 ± 50	361
$K^\pi = 2^+$		
$3_3^+ \rightarrow 2_3^+$	<590	298
$4_3^+ \rightarrow 2_3^+$	175_{-60}^{+100}	220
$4_3^+ \rightarrow 3_1^+$	$<785 \pm 650$	302

Figure 2.18 gives positive-parity energy curves with respect to the quadrupole deformation parameter β . We see, in addition to the minimum-energy point near $\beta = 0.2$ which corresponds to the ground band, the existence of the minimum-energy points near $\beta = 0.5$ which correspond to two superdeformed bands with $K^\pi = 0_2^+$ and $K^\pi = 2^+$. The calculated superdeformed bands have the wave function with $4\hbar\omega$ excitation (four particle jump from deformed sd to pf). The superdeformed state is triaxially deformed ($\gamma = 0.25$). In the case of the negative-parity energy curves, we see three minimum-energy points for $J^\pi = 1^-$ states with $K^\pi = 0^-$ in the low excitation energy region. The highest minimum-energy point is located near $\beta = 0.27$ and corresponds to the $^{40}\text{Ca} + \alpha$ cluster state. The other two minimum-energy points around $\beta = 0.25$ and 0.4 correspond to structures with dominantly $1\hbar\omega$ and $3\hbar\omega$ excitations, respectively. In Fig. 2.18 we give the density distributions of the intrinsic wave functions of the $J^\pi = 1^-$ state with $K^\pi = 0^-$ near $\beta = 0.27$. This density distribution clearly shows the $^{40}\text{Ca} + \alpha$ structure of this state. In this density distribution, the black points show the spatial positions of the centroids of the single-nucleon wave packets of AMD Slater determinant. While the nucleon wave packet centroids are divided clearly into two spatial groups for the $K^\pi = 0^-$ band, we do not see clear division of the nucleon wave packet centroids for the ground and $4\hbar\omega$ -jump bands. Thus the superdeformed states in ^{44}Ti are mean-field-type states and do not have clear clustering structure. It is reported in Ref. [88] that, if nucleon wave packets are not allowed to deform, the AMD wave function around the superdeformed deformation β has $^{36}\text{Ar} + 2\alpha$ structure.

In Table 2.11 we show the squared amplitudes W^J of the $^{40}\text{Ca} + \alpha$ component of the ground band states. The definition of W^J is given in Sect. 2.3.4.3. W^J values of the ground band are about 40% for low spin members which are fairly smaller

Table 2.11 Squared amplitudes of $^{40}\text{Ca} + \alpha$ component W^J and α spectroscopic factor S_α by AMD calculation [88]

J^π	W^J	S_α	$(S_\alpha)_{exp}$	J^π	W^J	S_α
[ground]				[$N = 14$]		
0^+	0.39	0.14	0.20	0^+	0.46	0.22
2^+	0.34	0.12	0.20	2^+	0.42	0.23
4^+	0.32	0.12	0.18	4^+	0.38	0.19
6^+	0.25	0.09	0.16	6^+	0.30	0.17
8^+	0.21	0.08	0.13	8^+	0.21	0.13
10^+	0.06	0.01		10^+	0.12	0.08
12^+	0.06	0.00				
[$N = 13$]				[$N = 15$]		
1^-	0.56	0.20	0.25	1^-	0.63	0.34
3^-	0.50	0.18	0.37	3^-	0.59	0.32
5^-	0.43	0.16	0.30	5^-	0.56	0.31
7^-	0.38	0.12		7^-	0.48	0.28
9^-	0.32	0.10		9^-	0.35	0.20

For ground and $N = 13$ bands S_α are compared with experiments

than the W^J values of the $^{16}\text{O} + \alpha$ component in the low spin members of the ground band of ^{20}Ne . But still they are of sizable magnitude in view of the density distributions of the ground band states which do not show clear clustering feature. For this sizable magnitude of W^J of the ground band, the following relation due to the Bayman–Bohr theorem makes a large contribution:

$$|^{40}\text{Ca}, (0f, 1p)^4; (12, 0)L\rangle = D_{L,\mathcal{A}} \left\{ R_{12,L}(r_{\text{Ca}-\alpha}, (40/11)v) Y_L(\hat{r}_{\text{Ca}-\alpha}) \phi(\alpha) \phi(^{40}\text{Ca}) \right\} \\ \times g(X_G, 40v). \quad (2.79)$$

The smaller W^J value of the $^{40}\text{Ca} + \alpha$ component in ^{44}Ti than the W^J value of the $^{16}\text{O} + \alpha$ component in ^{20}Ne is reasonable because the spin-orbit effect is much stronger than in ^{20}Ne and the core nucleus ^{40}Ca is much larger than the ^{16}O core in ^{20}Ne . As seen in the above equality due to the Bayman–Bohr theorem, the $^{40}\text{Ca} - \alpha$ relative wave functions contained in the ground band states have the value 12 for the quantum number $N = 2n + L$ with n standing for the number of nodes.

The percentage W^J of the $^{40}\text{Ca} + \alpha$ component of the $K^\pi = 0^-$ band which has $^{40}\text{Ca} + \alpha$ density distribution is larger than the ground band and is about 56% for the band head 1^- state but it decreases to about 32% for the 9^- state. The expectation value of the two-body spin-orbit force is -9.5 MeV for the ground state while it is -4.3 MeV for the band head 1^- state of the $K^\pi = 0^-$ band, which is the reflection of the smaller breaking of the spatial symmetry of the $K^\pi = 0^-$ band. The $^{40}\text{Ca} - \alpha$ relative wave functions contained in the $K^\pi = 0^-$ band states have the value 13 for the quantum number $N = 2n + L$, and hence in Table 2.11 this band is called the $N = 13$ band. In Table 2.11 we see good reproduction of the observed spectroscopic factor of $^{40}\text{Ca} + \alpha$ by AMD for the ground and $N = 13$ bands.

The AMD calculation gives excited bands with $K^\pi = 0^+$ and $K^\pi = 0^-$ which have $^{40}\text{Ca} + \alpha$ component with respective percentage numbers 46 and 63% for the band head 0^+ and 1^- states. The $^{40}\text{Ca} + \alpha$ components of these $K^\pi = 0^\pm$ bands have one more nodal points than the lower $K^\pi = 0^\pm$ bands in their $^{40}\text{Ca} - \alpha$ relative wave functions, namely $N = 14$ and 15 , respectively. Therefore, in Table 2.11 these bands are called the $N = 14$ and 15 bands, respectively. The $N = 14$ and 15 bands are called higher nodal $K^\pi = 0^\pm$ bands. In Ref. [80] the higher nodal $K^\pi = 0^\pm$ bands are reported to be observed experimentally, and they are shown in Fig. 2.17.

In the ground state of ^{44}Ti , the $^{40}\text{Ca} + \alpha$ component is contained by only about 40%. But the AMD calculation does not give any other 0^+ state which has larger percentage of $^{40}\text{Ca} + \alpha$ component with $N = 12$ below the higher nodal 0^+ state. Thus we are allowed to say that the parity inversion partner of the observed $K^\pi = 0^-$ band built upon the 1^- state around 7 MeV is the ground band. The higher nodal $K^\pi = 0^\pm$ bands can be regarded as the excited bands which are formed by the activation of the $^{40}\text{Ca} - \alpha$ clustering degree of freedom embedded in the ground band.

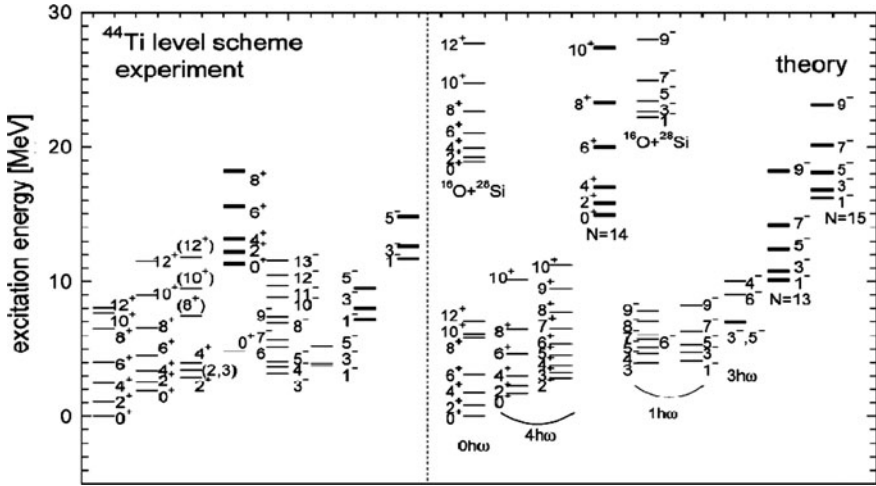


Fig. 2.17 Energy spectra of ^{44}Ti by AMD [88]. $(E_{th})_{exp}$ for $^{40}\text{Ca} + \alpha$ breakup is 5.14 MeV

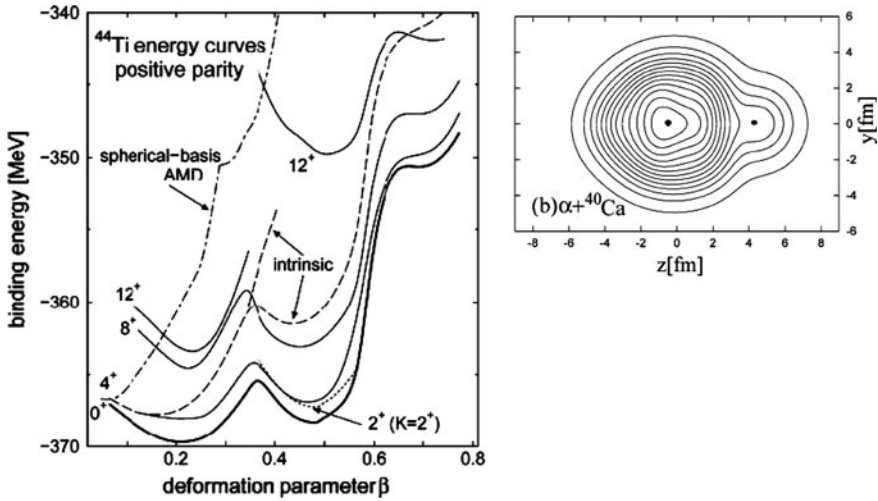


Fig. 2.18 Energy curves of positive-parity AMD states of ^{44}Ti with respect to quadrupole deformation and the density distribution of the intrinsic AMD wave function of the $J^\pi = 1^-$ state of $K^\pi = 0^-$ band [88]

2.4.2 ^{32}S Case

2.4.2.1 Superdeformed States and $^{16}\text{O} + ^{16}\text{O}$ Molecular Resonance States

In ^{32}S , many mean-field calculations predict the presence of the band with doubly superdeformed magic structure whose band head 0^+ state is located near

$E_x = 10$ MeV [89–91], although no definite experimental information has been obtained until now. The intrinsic state has a configuration with four nucleons raised into the deformed intruder orbit coming down from pf shell. The density distribution of this intrinsic state wave function looks like that of $^{16}\text{O} + ^{16}\text{O}$ molecular configuration. The microscopic study of the $^{16}\text{O} + ^{16}\text{O}$ molecular structure has been made by many authors [92–98], which is partly because the cluster system of two double-closed-shell nuclei is of fundamental importance and partly because the $^{16}\text{O} + ^{16}\text{O}$ molecular resonances were experimentally observed [99]. However, it was not easy to give any definite suggestion from microscopic theory to the $^{16}\text{O} + ^{16}\text{O}$ molecular resonance phenomena.

An important progress in the study of $^{16}\text{O} + ^{16}\text{O}$ system was made at the end of 80's, which was the discovery of the nuclear rainbow phenomena in the $^{16}\text{O} + ^{16}\text{O}$ elastic scattering [100]. This discovery made possible the derivation of unique $^{16}\text{O} - ^{16}\text{O}$ potential by Kondo and his coworkers [101, 102]. This unique potential proved to be deep contrary to the very shallow potentials long used to describe low energy scattering [99]. Additional measurements and calculations reinforced this deep potential picture for this $^{16}\text{O} - ^{16}\text{O}$ system [103–105] and neighboring systems like $^{12}\text{C} - ^{12}\text{C}$ and $^{12}\text{C} - ^{16}\text{O}$ [106]. Thus after years of controversy about the nature of the inter-nucleus potential, it is now definitely agreed that the potential is deep [17, 106, 107].

Recently it was argued, by calculating the eigenstates of the unique $^{16}\text{O} - ^{16}\text{O}$ potential, that the band of observed $^{16}\text{O} - ^{16}\text{O}$ molecular resonance states corresponds to the calculated rotational band having the number of $N = 2n + L = 28$ of the $^{16}\text{O} - ^{16}\text{O}$ relative motion with respect to the excitation energy [108] as shown in Fig. 2.19. Here n and L are the number of nodes and angular momentum of the relative wave function, respectively. Furthermore it was argued that the lowest rotational band having the lowest Pauli-allowed number of $N = 2n + L = 24$ has its band head 0^+ state at about 10 MeV in excitation energy (Fig. 2.19).

2.4.2.2 AMD Study of ^{32}S

AMD study of ^{32}S [109] teaches us how superdeformed states can be related to the molecular states. The AMD calculation by the use of the Gogny D1S force gives almost the same answer for the superdeformed excited rotational band as the Hartree–Fock calculations (Fig. 2.20). It is here to be noted that the minimum energy by the $^{16}\text{O} + ^{16}\text{O}$ Brink wave function is calculated to be higher by about 10 MeV than the superdeformed 0^+ . The Hill-Wheeler calculation by superposing the states on the AMD energy curve gives the refined superdeformed band and other two higher-lying rotational bands in addition to the ground state and low-lying excited states as shown in Fig. 2.21. The $^{16}\text{O} + ^{16}\text{O}$ component contained in the superdeformed band head state is about 42% and those contained in other two higher-lying rotational band head states

Fig. 2.19 Several lowest molecular bands calculated with unique $^{16}\text{O} - ^{16}\text{O}$ potential (circle points) [108]. *Filled triangle points* are averaged energy positions of observed $^{16}\text{O} + ^{16}\text{O}$ resonances. Observed angular distributions (*dots*) in the inset are from Ref. [99]

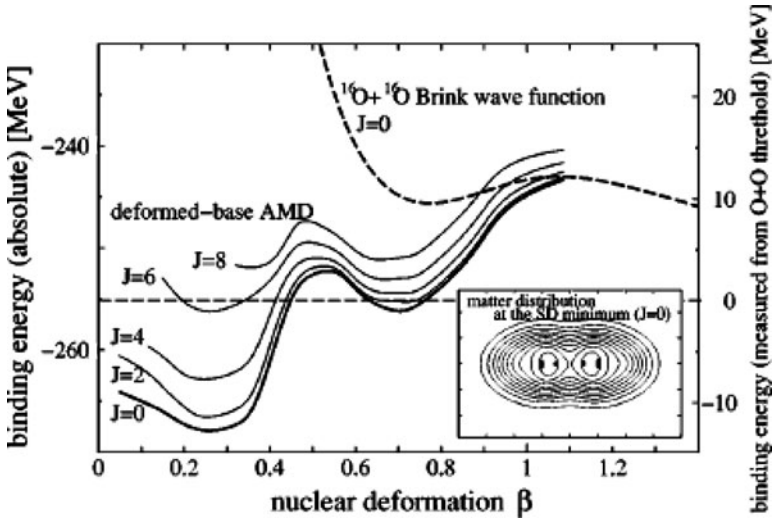
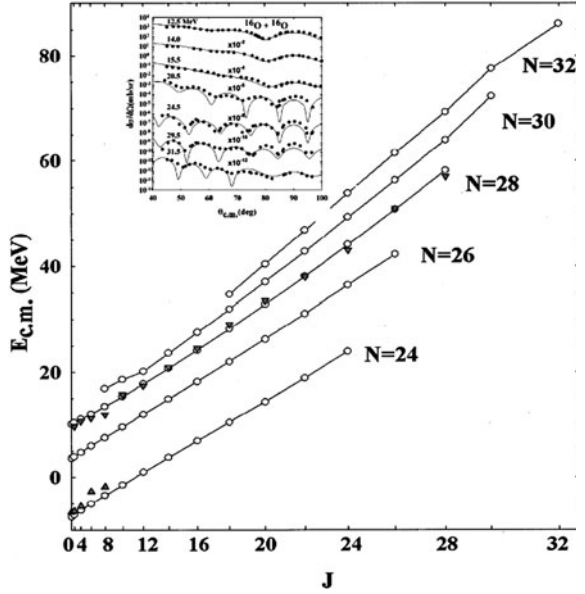
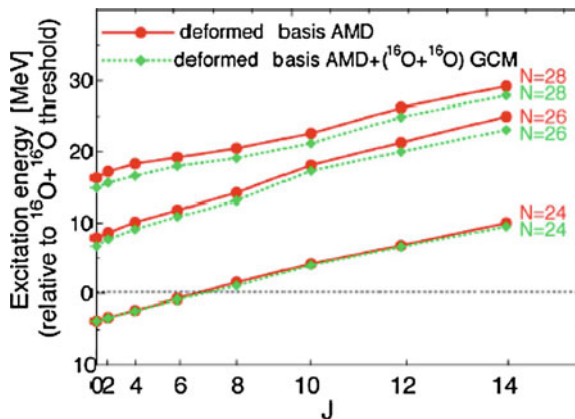


Fig. 2.20 Energy curves of ^{32}S with respect to quadrupole deformation by AMD [109]

are 71 and 73%. The expectation values of the two-body spin-orbit force are -4.5 , -3.2 , and -2.8 MeV for the superdeformed and two higher-lying band head states, respectively. The $^{16}\text{O} + ^{16}\text{O}$ components contained in the

Fig. 2.21 Superdeformed rotational band and two excited bands in ^{32}S by AMD [109]



superdeformed and high-lying bands have the $^{16}\text{O} - ^{16}\text{O}$ relative wave functions whose number of $N = 2n + L$ are 24, 26, and 28, respectively.

For the magnitude, about 42%, of the $^{16}\text{O} + ^{16}\text{O}$ component in the superdeformed band head state, the following relation due to the Bayman–Bohr theorem makes a large contribution:

$$\begin{aligned}
 & (0, 0, 0)^4 (1, 0, 0)^4 (0, 1, 0)^4 (0, 0, 1)^4 (1, 0, 1)^4 (0, 1, 1)^4 (0, 0, 2)^4 (0, 0, 3)^4 \\
 & = n \mathcal{A} \left\{ X_{(0,0,24)}(r_{\text{O-O}}, 8\nu) \phi(^{16}\text{O}) \phi(^{16}\text{O}) \right\} g(X_G, 32\nu).
 \end{aligned} \tag{2.80}$$

In Ref. [109] the Hill-Wheeler calculation was made in wider basis space by adopting $^{16}\text{O} + ^{16}\text{O}$ Brink wave functions in addition to the basis states on the AMD energy curve (Fig. 2.21). This improved Hill-Wheeler calculation gave only little change to the superdeformed band; the energy gain was very small and the percentage of the $^{16}\text{O} + ^{16}\text{O}$ component contained in the superdeformed band head state changed from about 42 to about 44%. However the improved Hill-Wheeler calculation gave rather large change to the two higher-lying bands, namely the percentages of the $^{16}\text{O} + ^{16}\text{O}$ components contained in these two band head states changed from about 71 and 73% to about 90 and 98%, respectively, although the energy gains for these two bands were rather small. The higher band with $N = 28$ is thus almost pure $^{16}\text{O} + ^{16}\text{O}$ molecular band.

When we compare three bands of AMD with $N = 24, 26$, and 28 with the three bands of unique $^{16}\text{O} - ^{16}\text{O}$ potential, we see good correspondence between them in excitation energies. Especially we can regard the AMD band with $N = 28$ as corresponding to the band of observed molecular resonances of $^{16}\text{O} + ^{16}\text{O}$. The AMD study teaches us that the $^{16}\text{O} + ^{16}\text{O}$ molecular resonance band is formed by the activation of the $^{16}\text{O} - ^{16}\text{O}$ clustering degree of freedom embedded in the superdeformed band.

2.5 Structure Change Between Cluster States and Mean-Field-Type States

2.5.1 Dual Character of Nuclear Wave Function

In previous sections we discussed the Bayman–Bohr theorem for the wave functions of the ground states of ^8Be , ^{12}C , ^{16}O , ^{20}Ne , and ^{44}Ti , and for that of the superdeformed excited state of ^{32}S . This theorem says that the nuclear many-body wave function possesses two faces, face of ‘mean-field-type structure’ and face of ‘cluster structure’. This fact may look like only a mathematical feature of the wave function. But it also represents a physical feature. It is because there do exist two kinds of excitation modes on the basis of this dual nature of the wave function. We below summarize what we discussed in previous sections in this lecture from this viewpoint.

In ^8Be we discussed Bayman–Bohr theorem for the ground state, but the ground state is a 2α cluster state rather than a mean-field-type state. In this nucleus, beyond the Bayman–Bohr theorem which compares the $\text{SU}(3)$ shell model wave function with the cluster model wave function, the deformed Hartree–Fock wave functions for several types of Skyrme forces were compared with the 2α cluster wave function [111]. The result showed that the Hartree–Fock wave functions contain a large amount of the 2α component (W' of Sect. 2.3.4.3) more than 97%. It is desirable to compare the Hartree–Fock wave functions with the optimum (minimum energy) 2α cluster wave function.

In ^{12}C , the ground state wave function is known to contain large amount of the $\text{SU}(3)$ shell model wave function $|(0s)^4(0p)^8, (\lambda, \mu) = (04)J = 0\rangle$. According to the Bayman–Bohr theorem, this wave function is equivalent to a 3α cluster wave function as follows,

$$\begin{aligned} |(0s)^4(0p)^8, (\lambda, \mu) = (04)J = 0\rangle \\ = N_0 \mathcal{A} \{ R_{4,0}(\xi_1, (8/3)v) R_{4,0}(\xi_2, 2v) \phi(\alpha_1) \phi(\alpha_2) \phi(\alpha_3) \} \quad (2.81) \\ \times g(X_G, 12v), \end{aligned}$$

where $\xi_1 = X_1 - (X_2 + X_3)/2$, $\xi_2 = X_2 - X_3$, and X_i stands for the center-of-mass coordinate of i th α cluster. Since the Hoyle state can be well described by the wave function $\mathcal{A} \{ P_A \exp(-(4/(3B^2))\xi_1^2 - (1/B^2)\xi_2^2) \phi(\alpha_1) \phi(\alpha_2) \phi(\alpha_3) \}$ with P_A standing for the projection operator onto the functional space having the number of oscillator quanta larger than 8, the formation of the Hoyle state can be regarded to be the excitation of the 3α relative wave function from $R_{4,0}(\xi_1, (8/3)v) R_{4,0}(\xi_2, 2v)$ of the ground state to $P_A \exp(-(4/(3B^2))\xi_1^2 - (1/B^2)\xi_2^2)$ of the Hoyle state. On the other hand, there is, of course, mean-field-type excitation of the ground state as is typically seen in the formation of the 1^+ excited state at 12.7 MeV having non-zero intrinsic spin $S = 1$.

In ^{16}O , it has been long known that the excited states of 3_1^- , 1_1^- , 2_1^- , 0_1^- , are dominantly of the structure of 1-particle 1-hole, namely they are the excited states due to the mean-field-type excitation mode. At the same time, as we described in section 3, it is now well known that lot of excited states including 0_2^+ , 2_1^+ , 2_2^+ , 4_1^+ , 6_1^+ , 1_2^- , 3_2^- , 5_1^- , 7_1^- , are dominantly of the cluster structure of $^{12}\text{C} + \alpha$ described by the wave function of the form $\mathcal{A}\{\chi_{\ell,L,J}(r_{C-\alpha})[Y_\ell(\hat{r}_{C-\alpha})\phi_L(^{12}\text{C})]_J\phi(\alpha)\}$. Since the Bayman–Bohr theorem assures that the double-closed-shell wave function of the ground state is equivalent to $^{12}\text{C} + \alpha$ cluster wave function as,

$$\begin{aligned} \det |(0s)^4(0p)^{12}| &= c_L \mathcal{A}\left[R_{4,L}(r_{C-\alpha}, 3\nu)\left[Y_L(\hat{r}_{C-\alpha})\phi_L(^{12}\text{C})\right]_{J=0}\phi(\alpha)\right] \\ &\times g(X_G, 16\nu), \end{aligned} \quad (2.82)$$

where L is arbitrary among $L = 0, 2$, and 4 , the formation of $^{12}\text{C} + \alpha$ cluster states can be regarded to be the excitation of the $^{12}\text{C} - \alpha$ relative motion from $R_{4,L}(r_{C-\alpha}, 3\nu)Y_L(\hat{r}_{C-\alpha})$ of the ground state to $\chi_{\ell,L,J}(r_{C-\alpha})Y_\ell(\hat{r}_{C-\alpha})$ of the cluster states.

In ^{20}Ne , the ground band states contain the $^{16}\text{O} + \alpha$ component at most 70%. This $^{16}\text{O} + \alpha$ component is mostly equivalent to SU(3) shell model wave function with $(\lambda, \mu) = (8, 0)$ due to Bayman–Bohr theorem (Eq. (2.61)):

$$\begin{aligned} |(0s)^4(0p)^{12}(1s, 0d)^4; (8, 0)L\rangle &= C_L \mathcal{A}\left\{R_{8,L}(r_{O-\alpha}, (16/5)\nu)Y_L(\hat{r}_{O-\alpha})\phi(^{16}\text{O})\phi(\alpha)\right\} \\ &\times g(X_G, 20\nu). \end{aligned} \quad (2.83)$$

We saw in Sect. 2.3 that the excitations of $^{16}\text{O} - \alpha$ clustering degree of freedom imbedded in the ground band states give rise to the excited cluster bands, $K^\pi = 0^-$ and $K^\pi = 0_4^+$ bands which are described by the wave functions of the form $\mathcal{A}\{\chi_L(r_{O-\alpha})Y_L(\hat{r}_{O-\alpha})\phi(^{16}\text{O})\phi(\alpha)\}$. On the other hand, in ^{20}Ne there exists the low-lying $K^\pi = 2^-$ band having mean-field-type structure. This band is dominantly formed by 1-particle 1-hole excitation of the ground state.

In ^{44}Ti , the ground band states contain the $^{40}\text{Ca} + \alpha$ component at most 40%. This $^{40}\text{Ca} + \alpha$ component is mostly equivalent to SU(3) shell model wave function with $(\lambda, \mu) = (12, 0)$ due to Bayman–Bohr theorem :

$$\begin{aligned} |^{40}\text{Ca}, (0f, 1p)^4; (12, 0)L\rangle &= D_L \mathcal{A}\left\{R_{12,L}(r_{Ca-\alpha}, (40/11)\nu)Y_L(\hat{r}_{Ca-\alpha})\phi(^{40}\text{Ca})\phi(\alpha)\right\} \\ &\times g(X_G, 40\nu). \end{aligned} \quad (2.84)$$

We saw in Sect. 2.4 that the excitations of $^{40}\text{Ca} - \alpha$ relative motion imbedded in the ground band give rise to the excited cluster bands, $K^\pi = 0^-$, and $N = 14, 15$ higher nodal bands which are described by the wave functions of the form $\mathcal{A}\{\chi_L(r_{Ca-\alpha})Y_L(\hat{r}_{Ca-\alpha})\phi(^{40}\text{Ca})\phi(\alpha)\}$. On the other hand, in ^{44}Ti there exists the low-lying $K^\pi = 3^-$ band having mean-field-type structure. This band is

dominantly formed by 1-particle 1-hole excitation of the ground state. Furthermore, there exist two low-lying superdeformed bands with mean-field-type structure formed by four-particle jump.

In ^{32}S we showed that the superdeformed band contains $^{16}\text{O} + ^{16}\text{O}$ component by about 44%. This $^{16}\text{O} + ^{16}\text{O}$ component is mostly equivalent to shell model wave function with 4p - 4h excitation due to Bayman–Bohr theorem :

$$(0, 0, 0)^4 (1, 0, 0)^4 (0, 1, 0)^4 (0, 0, 1)^4 (1, 0, 1)^4 (0, 1, 1)^4 (0, 0, 2)^4 (0, 0, 3)^4 \\ = n \mathcal{A} \left\{ X_{(0,0,24)}(r_{\text{O-O}}) \phi(^{16}\text{O}) \phi(^{16}\text{O}) \right\} g(X_G, 32\nu). \quad (2.85)$$

We explained that the excitation of $^{16}\text{O} - ^{16}\text{O}$ relative motion imbedded in the superdeformed band gives rise to the $^{16}\text{O} + ^{16}\text{O}$ molecular resonance band.

From these actual features of the coexistence of cluster states and mean-field-type states in ^{12}C , ^{16}O , ^{20}Ne , ^{44}Ti , and ^{32}S , one may say that the coexistence of cluster structure and mean-field-type structure is rather of logical necessity of the dual character of nuclear wave function. Recently this point has been argued by H. Horiuchi, K. Ikeda, K. Kato, and T. Yamada, who have called this dual nature of nuclear states the Janus nature of nuclei [110]. Of course this mechanism of the coexistence of mean-field type and cluster type states is based on the nature of nuclear force. Nuclear force has strong tensor force which gives rise to tightly bound alpha cluster and it is of course responsible to the formation of the mean field which is close to the harmonic oscillator field.

2.5.2 *E0 Transitions Between Ground State and Cluster States in ^{16}O and ^{12}C*

An important observable quantity which directly verifies the dual nature of the nuclear wave function expressed by the Bayman–Bohr theorem is the large strength of the monopole transition between shell model type ground state and the excited cluster states. $E0$ transition strengths between ground state and cluster states in light nuclei are actually strong in general with their order of magnitude comparable with single-nucleon strength [112, 113]. This looks strange because cluster states are many-particle many-hole states in the shell model description which implies $E0$ strengths from the ground state are much smaller than the single-nucleon strength.

Below we explain that the above problem of the $E0$ transition strength can be answered quite naturally by applying the Bayman–Bohr theorem to the ground state wave functions, by explicitly analysing the $E0$ transitions in ^{16}O and ^{12}C [113]. The observed strengths $M(E0)$ of the $E0$ transition in ^{16}O are 3.55, 4.03, and 3.3 fm² for $0_2^+ \leftrightarrow 0_1^+$, $0_3^+ \leftrightarrow 0_1^+$, and $0_5^+ \leftrightarrow 0_1^+$, respectively, while the observed $M(E0)$ in ^{12}C for $0_2^+ \leftrightarrow 0_1^+$ is 5.4 fm². A rough estimation of the single-nucleon strength $\langle u_f(r) | r^2 | u_i(r) \rangle$ is given by $(3/5)R^2$ with R standing for

the nuclear radius. This estimation is obtained under the uniform-density approximation of $u(r) \sim \sqrt{3/R^3}$ for $u_i(r)$ and $u_f(r)$. For $R \sim 3$ fm, we have $\langle u_f(r) | r^2 | u_i(r) \rangle \sim 5.4 \text{ fm}^2$. Another strange point, from shell model viewpoint, about the observed values of $M(E0)$ is the fact that the three excited 0^+ states of ^{16}O have very similar magnitude of $M(E0)$ although they have different complicated configurations of many-particle many-hole. The explanation given below also answers to this question.

2.5.2.1 $E0$ Transitions in ^{16}O

As we explained in Sect. 2.3, the 0_2^+ and 0_3^+ states can be dominantly described by $^{12}\text{C} + \alpha$ cluster model wave functions, $\mathcal{A}[\chi_0(r_{\text{C}-\alpha})[Y_0(\hat{r}_{\text{C}-\alpha})\phi_0(^{12}\text{C})]_{J=0}\phi(\alpha)]$ and $\mathcal{A}[\chi_2(r_{\text{C}-\alpha})[Y_2(\hat{r}_{\text{C}-\alpha})\phi_2(^{12}\text{C})]_{J=0}\phi(\alpha)]$, respectively. On the other hand, the ground state is dominantly described by the double-closed-shell wave function Φ_{DCS} which is equivalent to $\mathcal{A}[R_{4,L}(r_{\text{C}-\alpha}, 3\nu)[Y_L(\hat{r}_{\text{C}-\alpha})\phi_L(^{12}\text{C})]_{J=0}\phi(\alpha)]$ with arbitrary $L = 0, 2, 4$. Therefore the $E0$ transition between the ground state and a $^{12}\text{C} + \alpha$ cluster state is the transition between the relative wave function $R_{4,L}(r_{\text{C}} - \alpha, 3\nu)$ and $\chi_L(r_{\text{C}} - \alpha)$. Actually, in spite of the presence of the antisymmetrization, the $E0$ transition strength comes only from the relative motion part of the wave function. It means that the $E0$ transition strength comes only from the $E0$ operator $O(E0, \text{rel.})$ of the relative motion. In order to verify this, we decompose the total $E0$ operator $O(E0)$ between zero isospin states as

$$O(E0) = \frac{1}{2} \sum_{i=1}^{16} (r_i - X_G)^2 = O(E0, ^{12}\text{C}) + O(E0, \alpha) + O(E0, \text{rel.}), \quad (2.86)$$

$$O(E0, ^{12}\text{C}) = \frac{1}{2} \sum_{i \in ^{12}\text{C}} (r_i - X_{\text{C}})^2, \quad O(E0, ^{12}\text{C}) = \frac{1}{2} \sum_{i \in \alpha} (r_i - X_{\alpha})^2, \quad (2.87)$$

$$O(E0, \text{rel.}) = \frac{1}{2} \frac{12 \times 4}{16} r_{\text{C}-\alpha}^2. \quad (2.88)$$

We then note the fact that the relative wave function $\chi_L(r_{\text{C}} - \alpha)$ has the harmonic oscillator components whose number of the oscillator quanta is larger than 4 of $R_{4,L}(r_{\text{C}} - \alpha, 3\nu)$. From this fact we obtain the following equations,

$$\left\langle \Phi_{\text{DCS}} | \mathcal{A} \left\{ \chi_L(r_{\text{C}-\alpha}) \left[Y_L(\hat{r}_{\text{C}-\alpha}) O(E0, ^{12}\text{C}) \phi_L(^{12}\text{C}) \right]_{J=0} \phi(\alpha) \right\} \right\rangle = 0, \quad (2.89)$$

$$\left\langle \Phi_{\text{DCS}} | \mathcal{A} \left\{ \chi_L(r_{\text{C}-\alpha}) \left[Y_L(\hat{r}_{\text{C}-\alpha}) \phi_L(^{12}\text{C}) \right]_{J=0} O(E0, \alpha) \phi(\alpha) \right\} \right\rangle = 0. \quad (2.90)$$

In these equations use is made of the fact that the numbers of the oscillator quanta of $O(E0, ^{12}\text{C}) \phi_L(^{12}\text{C})$ and $O(E0, \alpha) \phi(\alpha)$ are not smaller than those of $\phi_L(^{12}\text{C})$ and

$\phi(\alpha)$, respectively, because both $\phi_L(^{12}\text{C})$ and $\phi(\alpha)$ have minimum numbers of oscillator quanta for ^{12}C and α nuclei, respectively. We thus obtain for the $M(E0)$

$$\begin{aligned} & \left\langle \Phi_{\text{DCS}} | O(E0) | \mathcal{A} \left\{ \chi_L(r_{C-\alpha}) \left[Y_L(\hat{r}_{C-\alpha}) \phi_L(^{12}\text{C}) \right]_{J=0} \phi(\alpha) \right\} \right\rangle \\ &= \left\langle \Phi_{\text{DCS}} | O(E0) | \mathcal{A} \left\{ O(E0, \text{rel.}) \chi_L(r_{C-\alpha}) \left[Y_L(\hat{r}_{C-\alpha}) \phi_L(^{12}\text{C}) \right]_{J=0} \phi(\alpha) \right\} \right\rangle. \end{aligned} \quad (2.91)$$

In Ref. [113], exact analytical formulas of $M(E0, 0_2^+ \rightarrow 0_1^+)$ and $M(E0, 0_3^+ \rightarrow 0_1^+)$ are obtained as

$$M(E0, 0_2^+ \rightarrow 0_1^+) = \frac{1}{2} \sqrt{\frac{\tau_{0,4}}{\tau_{0,6}}} \eta_6 \langle R_{40}(r, v) | r^2 | R_{60}(r, v) \rangle, \quad (2.92)$$

$$M(E0, 0_3^+ \rightarrow 0_1^+) = \frac{1}{2} \sqrt{\frac{\tau_{2,4}}{\tau_{2,6}}} \zeta_6 \langle R_{42}(r, v) | r^2 | R_{62}(r, v) \rangle, \quad (2.93)$$

$$\tau_{L,N} = \langle \Psi_{L,N} | \mathcal{A} \{ \Psi_{L,N} \} \rangle, \quad \Psi_{L,N} = R_{N,L}(r_{C-\alpha}, 3v) \left[Y_L(\hat{r}_{C-\alpha}) \phi_L(^{12}\text{C}) \right]_{J=0} \phi(\alpha), \quad (2.94)$$

$$|0_2^+\rangle = \sum_{N=6}^{\infty} \eta_N (C_N \mathcal{A} \{ \Psi_{0,N} \}), \quad ||C_N \mathcal{A} \{ \Psi_{0,N} \}|| = 1, \quad (2.95)$$

$$|0_3^+\rangle = \sum_{N=6}^{\infty} \zeta_N (D_N \mathcal{A} \{ \Psi_{2,N} \}), \quad ||D_N \mathcal{A} \{ \Psi_{2,N} \}|| = 1, \quad (2.96)$$

The quantity $\tau_{L,N}$ represents the effect of the antisymmetrization and actually is fairly smaller than unity in general for non large N . However, in the above analytical formulas, quantities $\tau_{L,N}$ appear in the form of ratio, $\tau_{0,4}/\tau_{0,6}$ and $\tau_{2,4}/\tau_{2,6}$, and the magnitudes of these ratios are close to unity, which implies that the effect of antisymmetrization has only little influence on the $M(E0)$ values. The quantities η_6 and ζ_6 are the coefficients of the $2\hbar\omega$ - jump component contained in $|0_2^+\rangle$ and $|0_3^+\rangle$, respectively, and their magnitudes are around 0.4. Note that η_6 and ζ_6 are not percentage quantities, $(\eta_6)^2$ and $(\zeta_6)^2$. The $E0$ matrix elements of the relative motion, $\langle R_{40}(r, v) | r^2 | R_{60}(r, v) \rangle$ and $\langle R_{42}(r, v) | r^2 | R_{62}(r, v) \rangle$, are larger than the corresponding $E0$ matrix elements of the single-nucleon motion, $\langle R_{00}(r, v) | r^2 | R_{20}(r, v) \rangle$ and $\langle R_{11}(r, v) | r^2 | R_{31}(r, v) \rangle$, by about 50%. We thus see that the order of magnitude of $M(E0, 0_2^+ \rightarrow 0_1^+)$ and $M(E0, 0_3^+ \rightarrow 0_1^+)$ are the same as the single-nucleon strength. Also we see that $M(E0, 0_2^+ \rightarrow 0_1^+)$ and $M(E0, 0_3^+ \rightarrow 0_1^+)$ should have similar magnitude because their analytical formulas are very similar each other.

The numerical values of $M(E0, 0_2^+ \rightarrow 0_1^+)$ and $M(E0, 0_3^+ \rightarrow 0_1^+)$ calculated with the above formulas with suitable parameter values are 1.97 fm² and 3.89 fm², respectively. These values are somewhat smaller than the observed values

although the order of magnitudes are reproduced. This problem was investigated in Ref. [113], and it was shown that the inclusion of the ground state correlation into the ground state wave function makes the reproduction of the observed values by theory fairly satisfactory. The ground state correlation adopted is the one due to the inter-cluster relative motion, namely the $^{12}\text{C} - \alpha$ relative wave function embedded in the ground state is not simply $R_{4,L}(r_C - \alpha, 3v)$ but has contributions from higher N components, $R_{N,L}(r_C - \alpha, 3v)$, with $N > 4$. The important point of this result is that the clustering degree of freedom described by the Bayman–Bohr theorem induces the ground state correlation which affects the $E0$ matrix elements.

2.5.2.2 $E0$ Transitions in ^{12}C

In Ref. [113] similar analytical formula of $M(E0)$ was derived for the transition between the ground state and the 0_2^+ state of ^{12}C (Hoyle state) as follows

$$M(E0, 0_2^+ \rightarrow 0_1^+) = \sqrt{\frac{7}{6}} \sqrt{\frac{\langle F_4 \rangle}{\langle F_5 \rangle}} \sigma_5 \langle R_{40}(r, v) | r^2 | R_{60}(r, v) \rangle, \quad (2.97)$$

$$\langle F_n \rangle = \langle Q_n | \mathcal{A} \{ Q_n \} \rangle, \quad Q_n = F_n(\xi_1, \xi_2) \phi(\alpha_1) \phi(\alpha_2) \phi(\alpha_3), \quad (2.98)$$

$$F_n(\xi_1, \xi_2) = \frac{1}{4\pi} \sum_{n_1+n_2=n} \sqrt{\frac{(2n_1+1)!!(2n_2+1)!!}{2n_1!!2n_2!!}} R_{2n_1,0}(\xi_1, (8/3)v) R_{2n_2,0}(\xi_2, 2v), \quad (2.99)$$

$$|0_2^+\rangle = \sum_{n=5}^{\infty} \sigma_n (e_n \mathcal{A} \{ Q_n \}), \quad ||e_n \mathcal{A} \{ Q_n \}|| = 1, \quad (2.100)$$

Here, as before, $|(0s)^4(0p)^8, (04)J=0\rangle$ was adopted as the ground state wave function, and $\mathcal{A}\{P_A \exp(-(4/(3B^2))\xi_1^2 - (1/B^2)\xi_2^2) \phi(\alpha_1) \phi(\alpha_2) \phi(\alpha_3)\}$ was adopted for the Hoyle state. Applying the Bayman–Bohr theorem to the ground state, the $E0$ transition is shown to be the transition of the 3α relative wave function between $R_{4,0}(\xi_1, (8/3)v)$, $R_{4,0}(\xi_2, 2v)$ and $P_A \exp(-(4/(3B^2))\xi_1^2 - (1/B^2)\xi_2^2)$ by the $E0$ operator of relative motion $O(E0, \text{rel.}) = (4/3)\xi_1^2 + \xi_2^2$.

The quantity $\langle F_n \rangle$ represents the effect of the antisymmetrization but in the above analytical formula, it appears in the form of ratio, $\langle F_4 \rangle / \langle F_5 \rangle$, whose magnitude is close to unity. Thus the effect of antisymmetrization has only little influence on the $M(E0)$ value like in the case of ^{16}O . The quantity σ_5 is the amplitude of the $2\hbar\omega$ -jump component contained in $|0_2^+\rangle$ and its magnitude is around 0.25. The $E0$ matrix element of the relative motion, $\langle R_{40}(r, v) | r^2 | R_{60}(r, v) \rangle$, is the same as in ^{16}O , and hence it is larger than the corresponding $E0$ matrix elements of the single-nucleon motion, $\langle R_{00}(r, v) | r^2 | R_{20}(r, v) \rangle$ and $\langle R_{11}(r, v) | r^2 | R_{31}(r, v) \rangle$, by about 50%. We thus

obtain the same result as in ^{16}O that the order of magnitude of $M(E0, 0_2^+ \rightarrow 0_1^+)$ is the same as the single-nucleon strength.

The numerical value of $M(E0, 0_2^+ \rightarrow 0_1^+)$ calculated with the above formula with suitable parameter values is 1.3 fm^2 . This value is smaller than the observed value although the order of magnitude is reproduced. In Ref. [113], there was given the same conclusion as in ^{16}O that the clustering degree of freedom described by the Bayman–Bohr theorem induces the ground state correlation which makes the magnitude of the calculated $E0$ matrix element close to the observed value.

2.6 Summary

(1) Actual features of coexistence of cluster states and mean-field-type states were discussed in six self-conjugate nuclei, ^8Be , ^{12}C , ^{16}O , ^{20}Ne , ^{44}Ti , and ^{32}S . (2) In many cases detailed studies with AMD were utilized. The existence of the nucleon spin alignment in higher spin members of rotational bands even with prominent clustering character is one of the interesting features of coexistence of cluster dynamics and mean-field-type dynamics. (3) Rather large percentage of clustering components in the ground bands of ^{20}Ne and ^{44}Ti (about 70 and 40% for ground states of ^{20}Ne and ^{44}Ti , respectively) and the superdeformed bands in ^{32}S (about 40% for band-head), is largely due to the Bayman–Bohr theorem. (4) All the excited states with cluster structure discussed in this lecture can be considered to be formed by the excitation of the clustering degrees of freedom embedded in the ground states (superdeformed state in ^{32}S) which is described by the Bayman–Bohr theorem. (5) An important evidence of the dual nature of ground state wave function described by the Bayman–Bohr theorem was shown to be given by the fact that lots of $E0$ transitions between cluster states and ground state in ^{16}O and ^{12}C are rather strong comparable to the single-nucleon strength. (6) Coexistence of cluster states and mean-field-type states was discussed to be rather of logical necessity due to the dual character of nuclear wave function.

References

1. H. Horiuchi, J. Phys. Conf. Ser. **111**, 012054 (2008)
2. Y. Kanada-En'yo, M. Kimura, H. Horiuchi, CDR Physique **4**, 497 (2003)
3. K. Wildermuth, W. McClure, *Springer Tracts in Modern Physics*, vol. 41, (Springer, Berlin, 1966)
4. K. Wildermuth, Y.C. Tang, *Unified Theory of the Nucleus, Clustering Phenomena in Nuclei*, Vieweg, Braunschweig (1977)
5. Y. Abe, Y. Akaishi, H. Bandō, J. Hiura, H. Horiuchi, K. Ikeda, M. Kamimura, T. Marumori, S. Nagata, F. Nemoto, Y. Suzuki, K. Takada, N. Takigawa, R. Tamagaki, H. Tanaka, Prog. Theor. Phys. Suppl. **52** (1972)

6. Y. Abe, Y. Fujiwara, H. Furutani, H. Horiuchi, K. Ikeda, M. Kamimura, K. Katō, H. Kanada, T. Kaneko, Y. Kondō, T. Matsuse, S. Nagata, H. Nishioka, S. Okabe, S. Saito, T. Sakuda, M. Seya, Y. Suzuki, A. Tohsaki-Suzuki, E. Uegaki, *Prog. Theor. Phys. Suppl.* **68** (1972)
7. H. Horiuchi, K. Ikeda, *International Review of Nuclear Physics*, vol. **4**, (World Scientific, Singapore, 1986), p. 1
8. W. von Oertzen, M. Freer, Y. Kanada-En'yo, *Phys. Rep.* **432**, 43 (2006)
9. A. Doté, H. Horiuchi, Y. Kanada-En'yo, *Phys. Rev. C* **56**, 1844 (1997)
10. Y. Kanada-En'yo, H. Horiuchi, *Prog. Theor. Phys. Suppl.* **142**, 205 (2001)
11. D.M. Brink, *Proceedings of the International School of Physics Enrico Fermi* **36** (Academic Press, New York, 1966), p. 247
12. B.F. Bayman, A. Bohr, *Nucl. Phys.* **9**, 596 (1958/1959)
13. S. Saito, *Prog. Theor. Phys.* **41**, 705 (1969)
14. S. Saito, *Prog. Theor. Phys. Suppl.* **62**, 11 (1977)
15. R. Tamagaki, H. Tanaka, *Prog. Theor. Phys.* **34**, 191 (1965)
16. I. Shimodaya, R. Tamagaki, H. Tanaka, *Prog. Theor. Phys.* **27**, 793 (1962)
17. H. Horiuchi, in *Trends in Theoretical Physics* vol. **2**, eds. by P.J. Ellis, Y.C. Tang (Addison-Wesley, Redwood, 1991), p. 277
18. Y. Funaki, H. Horiuchi, A. Tohsaki, P. Schuck, G. Röpke, *Prog. Theor. Phys.* **108**, 297 (2002)
19. R.B. Wiringa, S.C. Pieper, J. Carlson, V.R. Pandharipande, *Phys. Rev. C* **62**, 014001 (2000)
20. F. Hoyle, *Astrophys. J. Suppl.* **1**, 121 (1954)
21. C.W. Cook, W.A. Fowler, C.C. Lauritzen, T. Lauritzen, *Phys. Rev.* **107**, 508 (1957)
22. P. Navrátil, J.P. Vary, B.R. Barrett, *Phys. Rev. Lett.* **84**, 5728 (2000)
23. P. Navrátil, J.P. Vary, B.R. Barrett, *Phys. Rev. C* **62**, 054311 (2000)
24. H. Morinaga, *Phys. Rev.* **101**, 254 (1956)
25. H. Morinaga, *Phys. Lett.* **21**, 78 (1966)
26. Y. Suzuki, H. Horiuchi, K. Ikeda, *Prog. Theor. Phys.* **47**, 1517 (1972)
27. H. Horiuchi, *Prog. Theor. Phys.* **51**, 1266 (1974)
28. H. Horiuchi, *Prog. Theor. Phys.* **53**, 447 (1975)
29. Y. Fukushima, M. Kamimura, *Suppl. J. Phys. Soc. Jpn.* **44**, 225 (1978)
30. M. Kamimura, *Nucl. Phys. A* **351**, 456 (1981)
31. E. Uegaki, S. Okabe, Y. Abe, H. Tanaka, *Prog. Theor. Phys.* **57**, 1262 (1977)
32. E. Uegaki, Y. Abe, S. Okabe, H. Tanaka, *Prog. Theor. Phys.* **59**, 1031 (1978)
33. E. Uegaki, S. Okabe, Y. Abe, H. Tanaka, *Prog. Theor. Phys.* **62**, 1621 (1979)
34. Y. Kanada-En'yo, *Phys. Rev. Lett.* **81**, 5291 (1998)
35. T. Neff, H. Feldmeier, *Nucl. Phys. A* **738**, 357 (2004)
36. M. Chernykh, H. Feldmeier, T. Neff, P. von Neumann-Cosel, A. Richter, *Phys. Rev. Lett.* **98**, 032501 (2007)
37. A. Tohsaki, H. Horiuchi, P. Schuck, G. Röpke, *Phys. Rev. Lett.* **87**, 192501 (2001)
38. G. Röpke, A. Schnell, P. Schuck, P. Nozières, *Phys. Rev. Lett.* **80**, 3177 (1998)
39. Y. Funaki, A. Tohsaki, H. Horiuchi, P. Schuck, G. Röpke, *Phys. Rev. C* **67**, 051306 (2003)
40. S. Ali, A.R. Bodmer, *Nucl. Phys.* **80**, 99 (1966)
41. G.E. Brown, A.M. Green, *Nucl. Phys.* **75**, 401 (1966)
42. W.H. Bassichis, G. Ripka, *Phys. Lett.* **15**, 320 (1966)
43. A. Arima, H. Horiuchi, T. Sebe, *Phys. Lett. B* **24**, 129 (1967)
44. B. Roth, K. Wildermuth, *Nucl. Phys.* **20**, 10 (1960)
45. R.K. Sheline, K. Wildermuth, *Nucl. Phys.* **21**, 196 (1960)
46. H. Horiuchi, K. Ikeda, *Prog. Theor. Phys.* **40**, 277 (1968)
47. R.H. Davis, in *Proceedings of Third Conference on Reactions between Complex Nuclei*, eds. by A. Ghiorso, R.M. Diamond, H.E. Conzett (University of California Press, USA, 1963), p. 61
48. E.B. Carter, G.E. Mitchell, R.H. Davis, *Phys. Rev.* **133**, B1421 (1964)
49. E.B. Carter, G.E. Mitchell, R.H. Davis, *Phys. Rev.* **133**, B1434 (1964)
50. Y. Suzuki, *Prog. Theor. Phys.* **55**, 1751 (1976)

51. Y. Suzuki, Prog. Theor. Phys. **56**, 111 (1976)
52. H. Horiuchi, Prog. Theor. Phys. **51**, 745 (1974)
53. Y. Funaki, T. Yamada, H. Horiuchi, G. Röpke, P. Schuck, A. Tohsaki, Phys. Rev. Lett. **101**, 082502 (2008)
54. T. Yamada, P. Schuck, Eur. Phys. J. A. **26**, 185 (2005)
55. Y. Akiyama, A. Arima, T. Sebe, Nucl. Phys. A **138**, 273 (1969)
56. T. Inoue, T. Sebe, H. Hagiwara, A. Arima, Nucl. Phys. A **59**, 1 (1964)
57. K. Ikeda, N. Takigawa, H. Horiuchi, Prog. Theor. Phys. Suppl. **464** (1968)
58. F. Nemoto, Y. Yamamoto, H. Horiuchi, Y. Suzuki, K. Ikeda, Prog. Theor. Phys. **54**, 104 (1975)
59. Y. Kanada-En'yo, H. Horiuchi, Prog. Theor. Phys. **93**, 115 (1995)
60. M. Kimura, Phys. Rev. C **69**, 044319 (2004)
61. Y. Taniguchi, M. Kimura, H. Horiuchi, Prog. Theor. Phys. **112**, 475 (2004)
62. A. Bohr, B.R. Mottelson, *Nuclear Structure*, vol. II. (Benjamin, New York, 1975)
63. H. Horiuchi, Prog. Theor. Phys. Suppl. **62**, 90 (1977)
64. R. Bock, *Heavy Ion Collisions*, vol.1 (North Holland, Amsterdam, 1979)
65. R. Bock, *Heavy Ion Collisions*, vol.2, (North Holland, Amsterdam, 1980)
66. P. Braun-Munzinger, J. Barrette, Phys. Rep. **87**, 209 (1982)
67. C.E. Svensson, et al. Phys. Rev. Lett. **85**, 2693 (2000)
68. D. Rudolph, et al. Phys. Rev. C **65**, 034305 (2002)
69. E. Ideguchi, et al. Phys. Rev. Lett. **87**, 222501 (2001)
70. C.D. O'Leary, M.A. Bentley, B.A. Brown, D.E. Appelbe, R.A. Bark, D.M. Cullen, S. Ertürk, A. Maj, A.C. Merchant, Phys. Rev. C **61**, 064314 (2000)
71. H. Friedrich, K. Langanke, Nucl. Phys. A **252**, 47 (1975)
72. H. Kihara, M. Kamimura, A. Tohsaki-Suzuki, *Proceedings of International Conference on Nuclear Structure, Contributed Papers* (International Academic Printing, Tokyo, 1977), p. 234
73. A. Arima, *Proceedings of Topical Conference on Physics of Medium Light Nuclei* (Editrice Compositori, Bologna, 1978), p. 19
74. Th. Delbar, Gh. Grégoire, G. Paic, R. Ceuleneer, F. Michel, R. Vanderpoorten, A. Budzanowski, H. Dabrowski, L. Freindl, K. Garotowski, S. Micek, R. Planeta, A. Strzalkowski, K.A. Eberhard Phys. Rev. C **18**, 1237 (1978)
75. R. Ceuleneer, F. Michel, G. Reidemeister, Lect. Notes Phys. **156**, p. 227, (Springer, Berlin, 1982)
76. F. Michel, G. Reidemeister, S. Ohkubo, Phys. Rev. Lett. **57**, 1215 (1986)
77. F. Michel, S. Ohkubo, G. Reidemeister, Prog. Theor. Phys. Suppl. **132**, 7 (1998), Chapter 2 and references therein
78. T. Wada, H. Horiuchi, Phys. Rev. C **38**, 2063 (1988)
79. H. Horiuchi, Prog. Theor. Phys. **73**, 1172 (1985)
80. T. Yamaya, K. Katori, M. Fujiwara, S. Kato, S. Ohkubo, Prog. Theor. Phys. Suppl. **132**, 73 (1998), (Chapter 3 and references therein)
81. J.J. Simpson, W.R. Dixon, R.S. Storey, Phys. Rev. Lett. **31**, 946 (1973)
82. J.J. Kolata, J.W. Olness, E.K. Warburton, Phys. Rev. C **10**, 1663 (1974)
83. A. Arima, V. Gillet, J. Ginocchio, Phys. Rev. Lett. **25**, 16043 (1970)
84. D.C. Zheng, D. Berdichevsky, L. Zamick, Phys. Rev. C **38**, 437 (1988)
85. T. Inakura, S. Mizutori, M. Yamagami, K. Matsuyanagi, Nucl. Phys. A **710**, 261 (2002)
86. T. Yamada, S. Ohkubo, Z. Phys. A **349**, 363 (1994)
87. S. Ohkubo, Y. Hirabayashi, T. Sakuda, Phys. Rev. C **57**, 2760 (1998)
88. M. Kimura, H. Horiuchi, Nucl. Phys. A **767**, 58 (2006)
89. M. Yamagami, K. Matsuyanagi, Nucl. Phys. A **672**, 123 (2000)
90. H. Molique, J. Dobaczewski, J. Dudek, Phys. Rev. C **61**, 044304 (2000)
91. R.R. Rodríguez-Guzmán, J.L. Egido, L.M. Robledo, Phys. Rev. C **62**, 054308 (2000)
92. H. Friedrich, Nucl. Phys. A **224**, 537 (1974)
93. A. Tohsaki, F. Tanabe, R. Tamagaki, Prog. Theor. Phys. **53**, 1022 (1975)

94. T. Ando, A. Tohsaki, K. Ikeda, Prog. Theor. Phys. **64**, 1608 (1980)
95. D. Baye, G. Reidemeister, Nucl. Phys. A **258**, 157 (1976)
96. D. Baye, P.-H. Heenen, Nucl. Phys. A **276**, 354 (1977)
97. T. Wada, H. Horiuchi, Prog. Theor. Phys. **80**, 488 (1988)
98. T. Wada, H. Horiuchi, Prog. Theor. Phys. **80**, 502 (1988)
99. J.V. Maher, M.W. Sachs, R.H. Siemssen, A. Weidinger, D.A. Bromley, Phys. Rev. **188**, 1665 (1969)
100. E. Stiliaris, H.G. Bohlen, P. Fröbrich, B. Gebauer, D. Kolbert, W. von Oertzen, M. Wilpert, Th. Wilpert, Phys. Lett. **223B**, 291 (1989)
101. Y. Kondō, B.A. Robson, R. Smith, Phys. Lett. **227B**, 310 (1989)
102. Y. Kondō, F. Michel, G. Reidemeister, Phys. Lett. **242B**, 340 (1990)
103. D.T. Khoa, W. von Oertzen, A. Faessler, M. Ermer, H. Clement, Phys. Lett. **260B**, 278 (1991)
104. D.T. Khoa, W. von Oertzen, H.G. Bohlen, G. Bartnitzky, H. Clement, Y. Sugiyama, B. Gebaure, A.N. Ostrowski, Th. Wilpert, M. Wilpert, C. Langner, Phys. Rev. Lett. **74**, 34 (1995)
105. M.P. Nicoli, F. Haas, R.M. Freeman, N. Aissaoui, C. Beck, A. Elanique, R. Noucier, A. Morsad, S. Szilner, Z. Basrak, M.-E. Brandan, G.R. Satchler, Phys. Rev. C **61**, 064608 (1999)
106. M.-E. Brandan, G.R. Satchler, Phys. Rep. **285**, 143 (1997)
107. H. Horiuchi, in *Proceedings of IV International Conference on Clustering Aspects on Nuclear Structure and Nuclear Reactions*, eds. by J. S. Lilley and M. A. Nagarajan, (Reidel, Dordrecht, 1985), p. 35
108. S. Ohkubo, K. Yamashita, Phys. Rev. C **66**, 021301 (2002)
109. M. Kimura, H. Horiuchi, Phys. Rev. C **69**, 051304 (2004)
110. H. Horiuchi, Int. J. Mod. Phys. A **24**(11), 2205 (2009)
111. J.A. Maruhn, M. Kimura, S. Schramm, P.-G. Reinhard, H. Horiuchi, A. Tohsaki, Phys. Rev. C **74**, 044311 (2006)
112. T. Kawabata, H. Akimune, H. Fujita, Y. Fujita, M. Fujiwara, K. Hara, K. Hatanaka, M. Itoh, Y. Kanada-En'yo, S. Kishi, K. Nakanishi, H. Sakaguchi, Y. Shimbara, A. Tamii, S. Terashima, M. Uchida, T. Wakasa, Y. Yasuda, H.P. Yoshida, M. Yosoi, Phys. Lett. B **646**, 6 (2007)
113. T. Yamada, Y. Funaki, H. Horiuchi, K. Ikeda, A. Tohsaki, Prog. Theor. Phys. **120**, 1139 (2008)



<http://www.springer.com/978-3-642-13898-0>

Clusters in Nuclei

Volume 1

Beck, C. (Ed.)

2010, XII, 316 p. 158 illus., Softcover

ISBN: 978-3-642-13898-0